J. Fluid Mech. (2005), *vol.* 533, *pp.* 1–46.
doi:10.1017/S0022112005004088 Printed in the United Kingdom

Partitioning of particle velocities in gas–solid turbulent flows into a continuous field and a spatially uncorrelated random distribution: theoretical formalism and numerical study

By PIERRE FÉVRIER[1,2]†, OLIVIER SIMONIN[1] AND KYLE D. SQUIRES[2]

[1]Institut de Mécanique des Fluides; UMR 5502 CNRS/INPT/UPS Allée du Professeur Camille Soula, 31400 Toulouse, France

[2]Mechanical and Aerospace Engineering, Box 876106, Arizona State University, Tempe, Arizona 85257-6106, USA

(Received 30 June 2003 and in revised form 4 January 2005)

The velocity distribution of dilute suspensions of heavy particles in gas–solid turbulent flows is investigated. A statistical approach – the mesoscopic Eulerian formalism (MEF) – is developed in which an average conditioned on a realization of the turbulent carrier flow is introduced and enables a decomposition of the instantaneous particle velocity into two contributions. The first is a contribution from an underlying continuous turbulent velocity field shared by all the particles – the mesoscopic Eulerian particle velocity field (MEPVF) – that accounts for all particle–particle and fluid–particle two-point correlations. The second contribution corresponds to a distribution – the quasi-Brownian velocity distribution (QBVD) – that represents a random velocity component satisfying the molecular chaos assumption that is not spatially correlated and identified with each particle of the system. The MEF is used to investigate properties of statistically stationary particle-laden isotropic turbulence. The carrier flow is computed using direct numerical simulation (DNS) or large-eddy simulation (LES) with discrete particle tracking employed for the dispersed phase. Particle material densities are much larger than that of the fluid and the force of the fluid on the particle is assumed to reduce to the drag contribution. Computations are performed in the dilute regime for which the influences of inter-particle collisions and fluid-turbulence modulation are neglected. The simulations show that increases in particle inertia increase the contribution of the quasi-Brownian component to the particle velocity. The particle velocity field is correlated at larger length scales than the fluid, with the integral length scales of the MEPVF also increasing with particle inertia. Consistent with the previous work of Abrahamson (1975), the MEF shows that in the limiting case of large inertia, particle motion becomes stochastically equivalent to a Brownian motion with a random spatial distribution of positions and velocities. For the current system of statistically stationary isotropic turbulence, both the DNS and LES show that the fraction of the kinetic energy residing in the mesoscopic field decreases with particle inertia as the square root of the ratio of the total particulate-phase kinetic energy to that of the fluid.

† Present address: Michelin, Place des Carmes-Déchaux, 63040 Clermont Ferrand Cedex 9, France, p.fevrier@libertysurf.fr

1. Introduction

The dynamical evolution of small heavy particles suspended in turbulent flows continues to receive attention because of its relevance to technologies governing a broad range of industrial and naturally occurring systems. Examples include the combustion of pulverized coal or liquid sprays, transport of particulate solids, gas-phase reactions controlled by particulate catalysts, dust storms, and atmospheric dispersal of pollutants. In each of these areas an increased understanding of the phenomena that drive the interactions between the particle cloud and turbulence is needed to ultimately improve the design of engineering devices in which these flows occur.

An overview of some of the important mechanisms governing turbulent gas–solid flows has been provided by Sommerfeld (2000), summarizing complex interactions governing particle transport by fluid turbulence, preferential concentration, inter-particle and wall–particle collisions, and two-way coupling. As described by Sommerfeld (2000), particle inertia plays an important role, as it dictates the interactions between the particle and turbulent scales of the carrier flow over the entire spectrum of length and time scales. Relevant to the present contribution are investigations of the spatial features of the particulate phase, which appear useful in understanding and modelling many of the important processes governing turbulent two-phase flows.

Much previous work in gas–solid turbulent flows has focused on the interactions between the continuous and dispersed phases that result in significant structure of the number density field. Structural interactions that lead to preferential concentration of particles into regions of low vorticity and/or high strain rate, for example, can influence the statistics of the particulate phase. Février (2000) showed a correlation between the local instantaneous distribution of inertial particles and the turbulent fluid velocity field that results in an increase in the fluid Lagrangian integral time scale sampled along the particle path. This in turn leads to a greater dispersion of heavy particles at long diffusion times compared to the fluid. Particle settling in isotropic turbulence provides another example in which the increase in the settling velocity of small heavy particles is directly connected to the correlation between the spatial distribution of the particles and the fluid velocity (Maxey 1987; Wang & Maxey 1993).

In addition to transport, inter-particle collisions and turbulence modulation by particles in dilute gas–solid flows provide other examples in which the spatial characteristics of the particle distribution are important in increasing understanding and developing improved phenomenological models. Previous studies have shown that structure in the particle number density (e.g. preferential concentration) has an important effect on collision rates in gas–solid flows (e.g. see Sundaram & Collins 1997; Wang, Wexler & Zhou 2000; Reade & Collins 2000). These and other studies show that preferential concentration resulting in locally large number densities increases collision rates over that which would be obtained for a random particle distribution. Sundaram & Collins (1997) accounted for the influence of the spatial distribution on collision frequencies via introduction of the radial distribution function at contact (see also Wang *et al.* 2000).

In regimes of significant mass loading such that the carrier flow is modified by momentum exchange with the particles, spatial characteristics of the particle distribution again appear to be an important factor. Previous numerical simulations using simple force-coupling models indicate that the distribution of particles in the flow can have a strong effect on the spectral content of the fluid turbulence. Simulations of isotropic turbulence have shown a non-uniform attenuation of the fluid energy spectrum for

parameter combinations in which there are strong structural interactions between the particles and turbulent fluid flow (Squires & Eaton 1991*a*; Elghobashi & Truesdell 1993; Boivin, Simonin & Squires 1998; Sundaram & Collins 1999).

1.1. *The partitioning effect of particle inertia*

Important to the present contribution is that interactions between the dispersed and continuous phases not only structure the particle number density, but also lead to correlation of the velocities of neighbouring particles. As discussed in Abrahamson (1975), it seems legitimate to assume that the two-particle velocity distribution will have the following asymptotic behaviours. For small-inertia particles, neighbouring velocities will be spatially correlated through the interactions with the same local fluid flow, an effect apparent in the velocity vectors of small-inertia particles shown in figure 1(*a*). The figure shows a single plane from calculation of particle-laden isotropic turbulence with the gas-phase computed using direct numerical simulation (DNS) and Lagrangian tracking for the dispersed phase (details of the calculation are presented in § 4).

In contrast, for large-inertia particles with response times that are long compared to the fluid turbulence macroscales, neighbouring particle velocities are uncorrelated since these particles maintain a stronger connection (memory) to their interactions with very distant, and independent, turbulent eddies. This effect is illustrated in figure 1(*b*) in which velocity vectors of large-inertia particles are shown in the same plane and at the same instant as for the low-inertia particles in figure 1(*a*). As the figure shows, velocity vectors of neighbouring particles appear uncorrelated. In the large-inertia limit, statistics of the particle velocity distribution will satisfy the assumption of molecular chaos and can be described using kinetic theory (e.g. see Reeks 1977). An important consequence is that in the large-inertia limit, the particle velocity distribution cannot be assumed to correspond to a spatially continuous velocity field. The random nature of the particle motion will lead to a crossing of individual trajectories (obviously inducing a collision in physical systems).

The above small- and large-inertia limit cases illustrate that substantially different spatial features in the particle velocity are possible, with these differences depending on particle inertia. In the scalar limit, the spatial correlation function between any two particle velocities should be accurately modelled by a decaying exponential, analogous to the correlation describing the fluid turbulence (Hinze 1975). On the other hand, in the limit of very large inertia particle motion becomes stochastically equivalent to a Brownian motion with independent random velocities, even for those particles passing close to each other (Abrahamson 1975; Reeks 1977). For intermediate values of the particle response time, the particle velocity distribution should be expected to exhibit spatial features with characteristics representative of these two limiting regimes.

In order to develop an improved understanding of the physical mechanisms associated with the rather different particle dynamics depicted in each limiting case illustrated above, an approach is developed in this manuscript based on the conjecture that *in dilute gas–solid turbulent flows, spatial velocity correlation between separate particles is only induced via particle interactions with the turbulent fluid motion. Specifically, inter-particle collisions or hydrodynamic interactions are assumed to not induce any correlation between the velocities of neighbouring particles.*

The approach – the mesoscopic Eulerian formalism (MEF) – is based on the presumed chaotic behaviour of inertial particles interacting with a given realization of the gas-phase turbulence. Indeed, it is assumed that small deviations in the initial conditions of the particles (position and velocity) are quickly magnified. For finite time

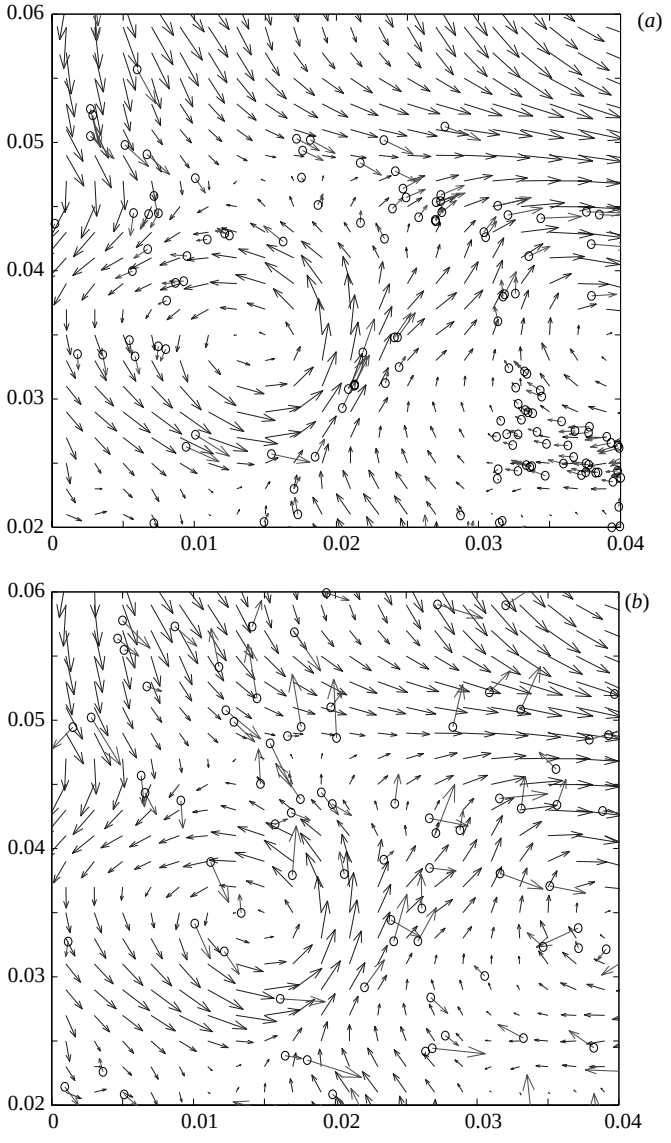

FIGURE 1. Instantaneous fluid and particle velocity vectors from a single plane of a direct numerical simulation of forced isotropic turbulence with Lagrangian particle tracking (see § 4). The longitudinal integral length scale of the fluid turbulence is $L_F^f \approx 0.02 L_{box}$. (*a*) Particle relaxation time is $0.13 T_L$ where T_L is the fluid Lagrangian integral timescale. (*b*) Particle relaxation time is $2.17 T_L$. In both (*a*) and (*b*) the particle positions are shown by the circles, the symbol size in each frame and particle velocity vectors in (*b*) are exaggerated for clarity.

typically larger than the particle response time and the fluid turbulence time macroscale, statistical properties of the dispersed phase, including the spatial correlations between neighbouring particles, become independent of the initial conditions and will be fully controlled by the interactions with the turbulent fluid flow. This chaotic behaviour of the particles in a given realization of the turbulent flow is connected to the case of fluid elements, e.g. as discussed in Falkovich, Gawedzki & Vergassola (2001), though this feature should be enhanced due to particle inertia (e.g. see

Wang, Burton & Stock (1991). Indeed, for small separations, even smaller than the Kolomogorov length scale, particle inertia should maintain the influence of the interactions with fluid elements at larger separation which are only partially correlated. Thus, multiple particle trajectories can pass through the same point at the same time for the given fluid flow realization.

1.2. *Objective and overview*

The main objective of the present study is to develop a more thorough understanding of the particle velocity spatial distribution. The focus of this effort is on gas–solid turbulent flows with a mono-disperse distribution of particles with material densities much larger than the fluid ($\rho_p \gg \rho$) and with particle diameters smaller than the smallest turbulent length scales of the fluid flow. Particle concentrations are dilute, effects of turbulence modulation and inter-particle collision are not within the scope of this study, and an extension of the approach developed in this manuscript to account for collisional effects and two-way coupling is summarized in the conclusion.

The approach is based on analysis and numerical simulation. In the first part of the manuscript a theoretical formalism is introduced to describe the local and instantaneous particle dynamics in an Eulerian frame of reference – referred to as the mesoscopic Eulerian formalism (MEF). In the second part of the paper, the MEF is used to study the spatial properties of the particle velocity distribution. The computations are based on direct numerical simulation (DNS) or large-eddy simulation (LES) of statistically stationary isotropic turbulence and with a Lagrangian treatment of the dispersed phase.

The analysis in Part I (§§2 and 3) based on the mesoscopic Eulerian formalism is a systematic approach that enables assessment of two contributions to the particle velocity field:

1. A turbulent contribution from an underlying continuous velocity field of the particulate phase that is local and time-dependent. This velocity is described in Eulerian coordinates and referred to as the mesoscopic Eulerian particle velocity field (MEPVF). The MEPVF is shared by all the particles and accounts for interactions with the entire spectrum of fluid turbulent motions.

2. A velocity distribution satisfying the assumption of molecular chaos, i.e. not correlated in space, and referred to as the quasi-Brownian velocity distribution (QBVD). A Lagrangian coordinate system is appropriate for the QBVD as it is associated with each particle separately.

Analytical relations involving the MEPVF and QBVD are derived and among the important results developed is that the MEPVF accounts for all particle–particle and fluid–particle two-point velocity correlations, while the QBVD is not correlated spatially, neither between separate particles, nor with the fluid velocity field. Thus, the approach presented in the first part of the paper formally shows that a portion of the particle velocity corresponds to a distribution that satisfies, partially, the assumption of molecular chaos, i.e. neighbouring particle velocities are completely independent. In the current context, the 'molecular chaos assumption' refers only to the velocity distribution, not the distribution of particle positions and also does not imply a Gaussian distribution of the particle velocities.

Following the development of the analytical relations, results from numerical simulations of statistically stationary, particle-laden isotropic turbulence are presented. The simulations are based on DNS and LES of the gas-phase turbulent carrier flow and Lagrangian calculation of the particle trajectories. A numerical approach is introduced in order to perform an *a priori* application of the MEF. Important in this

process is validation of the numerical procedures in order to accurately analyse the MEPVF and the QBVD, as well as one- and two-point statistics of the particulate flow. The numerical simulations are used to investigate the influence of particle inertia on properties of the particle velocity distribution. Transport equations that describe the evolution of the MEPVF are derived and used to shed light on properties of the particle velocity field; one of the important outcomes is that the transport equations for the MEPVF contain a contribution from the quasi-Brownian field via a kinetic stress tensor. This tensor represents diffusion and pressure corresponding to the important physical characteristic that within any volume Ω having dimensions comparable with or smaller than the smallest length scales of the turbulence, separate particles will possess different velocities because of separate fluid interaction histories.

Part I. Development of the Mesoscopic Eulerian Formalism

2. Background

In this section, statistics of the particle velocity distribution are developed, both for the Lagrangian temporal correlation and Eulerian two-point (spatial) correlation. The purpose is to illustrate the effect of particle inertia using conventional single-particle (in time) and two-particle (in space) measures. This overview will highlight the two contributions to the particle velocity distribution, one coming from a spatially correlated and continuous velocity field possessed by all the particles and the other a random contribution associated separately with each particle. This overview provides the context for the work and motivation for considering the spatial characteristics of the particle velocity distribution in turbulent flows and, in particular, the framework for development of the mesoscopic Eulerian formalism in § 3. The results presented in this section have been obtained from large-eddy simulations of statistically stationary, isotropic turbulence for the fluid together with Lagrangian calculation of particle trajectories. Details of the calculations are provided in Part II of the manuscript (§§ 4–6).

2.1. *Statistical descriptors of the particle velocity distribution*

The particle-phase system is classically described in terms of the one-particle probability distribution function (p.d.f.) $f_p^{(1)}(\boldsymbol{x}, \boldsymbol{c}_p, t)$ defining the local probable number of particle centres at the position $\boldsymbol{x}$, with a given translation velocity $\boldsymbol{v}_p = \boldsymbol{c}_p$, at time t. The p.d.f. $f_p^{(1)}$ can be obtained by ensemble averaging over a very large number, $\mathscr{N}_{f\&p}$, of two-phase flow realizations, $\mathscr{H}_{f\&p}$,

$$f_p^{(1)}(\boldsymbol{x}, \boldsymbol{c}_p, t) = \lim_{\mathscr{N}_{f\&p}\to\infty} \left[\frac{1}{\mathscr{N}_{f\&p}} \sum_{\mathscr{N}_{f\&p}} \sum_{m=1}^{N_p} W_p^{(m)}(\boldsymbol{x}, \boldsymbol{c}_p, t, \mathscr{H}_{f\&p}) \right] \tag{2.1}$$

where $W_p^{(m)}(\boldsymbol{x}, \boldsymbol{c}_p, t, \mathscr{H}_{f\&p}) = \delta(\boldsymbol{x} - \boldsymbol{x}_p^{(m)}(t))\delta(\boldsymbol{c}_p - \boldsymbol{v}_p^{(m)}(t))$ is the so-called refined-grid p.d.f. (e.g. see Reeks 1991), $\delta(a)$ is the Dirac function, and N_p is the (fixed) number of particles in any realization.

Using $f_p^{(1)}$, single-point macroscopic quantities can be defined. The mean particle number density is

$$n_p(\boldsymbol{x}, t) = \int f_p^{(1)}(\boldsymbol{x}, \boldsymbol{c}_p, t)\, \mathrm{d}\boldsymbol{c}_p, \tag{2.2}$$

and the mean particle velocity is

$$V_{p,i}(\boldsymbol{x}, t) = \frac{1}{n_p(\boldsymbol{x}, t)} \int c_{p,i} f_p^{(1)}(\boldsymbol{x}, \boldsymbol{c}_p, t)\, \mathrm{d}\boldsymbol{c}_p. \tag{2.3}$$

Note that, as particles within the system are indistinguishable, it is also possible to use the normalized probability distribution function $\mathscr{F}_p^{(1)}(\boldsymbol{x}, \boldsymbol{c}_p, t)$ computed for any given particle m from the realizations $\mathscr{N}_{f\&p}$,

$$\mathscr{F}_p^{(1)}(\boldsymbol{x}, \boldsymbol{c}_p, t) = \lim_{\mathscr{N}_{f\&p}\to\infty} \left[\frac{1}{\mathscr{N}_{f\&p}} \sum_{\mathscr{N}_{f\&p}} W_p^{(m)}(\boldsymbol{x}, \boldsymbol{c}_p, t, \mathscr{H}_{f\&p}) \right]. \tag{2.4}$$

These two statistical descriptions are obviously linked via $f_p^{(1)} = N_p \mathscr{F}_p^{(1)}$. In this paper statistics will be defined using both the p.d.f. $f_p^{(1)}$ and $\mathscr{F}_p^{(1)}$. Using the normalized p.d.f. the mean particle velocity is then

$$\begin{aligned} V_{p,i}(\boldsymbol{x}, t) &= \frac{\left\langle v_{p,i}^{(m)}(t) \delta\left(\boldsymbol{x} - \boldsymbol{x}_p^{(m)}(t)\right)\right\rangle}{\left\langle \delta\left(\boldsymbol{x} - \boldsymbol{x}_p^{(m)}(t)\right)\right\rangle} \\ &= \left\langle v_{p,i}^{(m)}(t) | \boldsymbol{x} = \boldsymbol{x}_p^{(m)}(t)\right\rangle, \end{aligned} \tag{2.5}$$

where the velocity of particle m is denoted $v_{p,i}^{(m)}(t)$ and the second line is a shorthand used to reinforce the dependence of the average on the particle position. The averaging operator $\langle\cdot\rangle$ is defined over a large number of two-phase flow realizations,

$$\langle\cdot\rangle = \lim_{\mathscr{N}_{f\&p}\to\infty} \left[\frac{1}{\mathscr{N}_{f\&p}} \sum_{\mathscr{N}_{f\&p}} (\cdot) \right]. \tag{2.6}$$

Note that when there is no ambiguity a simpler notation than introduced above can be used to denote averages, e.g. as taken with respect to a 'test particle' having velocity $\boldsymbol{v}_p$ and position $\boldsymbol{x}_p$. This notation is used in the following and, for example, the mean particle velocity is then expressed as

$$V_{p,i}(\boldsymbol{x}, t) = \langle v_{p,i}(t) | \boldsymbol{x} = \boldsymbol{x}_p(t)\rangle. \tag{2.7}$$

The fluctuating particle velocity vector is defined as

$$\boldsymbol{v}'_p(t) = \boldsymbol{v}_p(t) - \boldsymbol{V}_p(\boldsymbol{x}_p(t), t). \tag{2.8}$$

Using the above relations, the macroscopic particle kinetic energy is

$$q_p^2(\boldsymbol{x}, t) = \tfrac{1}{2}\langle v'_{p,i}(t) v'_{p,i}(t) | \boldsymbol{x} = \boldsymbol{x}_p(t)\rangle, \tag{2.9}$$

the fluid–particle velocity covariance, defined from the fluid velocity fluctuation at the particle location, is

$$q_{fp}(\boldsymbol{x}, t) = \langle u'_i(\boldsymbol{x}, t) v'_{p,i}(t) | \boldsymbol{x} = \boldsymbol{x}_p(t)\rangle, \tag{2.10}$$

and the fluid turbulent kinetic energy sampled along the particle trajectory is

$$q_{f@p}^2(\boldsymbol{x}, t) = \tfrac{1}{2}\langle u'_i(\boldsymbol{x}, t) u'_i(\boldsymbol{x}, t) | \boldsymbol{x} = \boldsymbol{x}_p(t)\rangle. \tag{2.11}$$

Note that the fluid velocity u'_i is defined at the particle centre and represents the value undisturbed by the presence of the particle but accounts for the disturbances created by the other particles in the system as well as the underlying turbulent motion of the carrier fluid.

The above measures are typical quantities extracted from one-particle p.d.f.s and used to analyse some of the main features of particle motion in turbulent flows. For two-point correlations, Sundaram & Collins (1994, 1999) developed a two-field formalism to calculate two-point correlations and corresponding spectral densities. The generic two-point correlations involve two contributions arising from intra-particle correlations and inter-particle correlations, taking into account the particle diameter. The inter-particle correlation is a function of the location of the centres of two separate particles and then defined for particle separations larger than the particle diameter. In the present manuscript, attention is restricted to two-point correlations conditioned by the particle centres, i.e. only inter-particle correlations are considered. To assess the two-point statistics of the particle phase, the probability distribution function $f_p^{(2)}$ associated with the motion of the centres of any two separate particles is considered,

$$f_p^{(2)}(\boldsymbol{x}, \boldsymbol{c}_p, \boldsymbol{x}^+, \boldsymbol{c}_p^+, t) = \lim_{\mathscr{N}_{f\&p}\to\infty} \left[\frac{1}{\mathscr{N}_{f\&p}} \sum_{\mathscr{N}_{f\&p}} \sum_{m=1}^{N_p} \sum_{n=1}^{N_p} W_p^{(m,n)}(\boldsymbol{x}, \boldsymbol{c}_p, \boldsymbol{x}^+, \boldsymbol{c}_p^+, t, \mathscr{H}_{f\&p}) \right], \tag{2.12}$$

where $W_p^{(m,n)}$ is the refined-grid p.d.f. for the motion of two particles m and n ($m \neq n$),

$$\begin{aligned} W_p^{(m,n)}(\boldsymbol{x}, \boldsymbol{c}_p, \boldsymbol{x}^+, \boldsymbol{c}_p^+, t, \mathscr{H}_{f\&p}) = {} & \delta\big(\boldsymbol{x} - \boldsymbol{x}_p^{(m)}(t)\big)\delta\big(\boldsymbol{c}_p - \boldsymbol{v}_p^{(m)}(t)\big) \\ & \times \delta\big(\boldsymbol{x}^+ - \boldsymbol{x}_p^{(n)}(t)\big)\delta\big(\boldsymbol{c}_p^+ - \boldsymbol{v}_p^{(n)}(t)\big). \end{aligned} \tag{2.13}$$

Note that the pair probability distribution $f_p^{(2)}(\boldsymbol{x}, \boldsymbol{c}_p, \boldsymbol{x}^+, \boldsymbol{c}_p^+, t)$ is restricted to separate particles and consequently the summation in (2.12) written for $m \neq n$.

As for the one-particle statistical description, two-particle statistics can be analogously defined from the normalized probability distribution function $\mathscr{F}_p^{(2)}$,

$$\mathscr{F}_p^{(2)}(\boldsymbol{x}, \boldsymbol{c}_p, \boldsymbol{x}^+, \boldsymbol{c}_p^+, t) = \lim_{\mathscr{N}_{f\&p}\to\infty} \left[\frac{1}{\mathscr{N}_{f\&p}} \sum_{\mathscr{N}_{f\&p}} W_p^{(m,n)}(\boldsymbol{x}, \boldsymbol{c}_p, \boldsymbol{x}^+, \boldsymbol{c}_p^+, t, \mathscr{H}_{f\&p}) \right], \tag{2.14}$$

from which follows $f_p^{(2)} = N_p(N_p - 1)\mathscr{F}_p^{(2)}$.

The two-point velocity correlations of any two (separate) particles of the system can now be defined using the two-particle p.d.f. (2.12). The reader is referred to the detailed expressions in the Appendix. The particle–particle velocity correlation is expressed as

$$R_{ij}^{pp}(\boldsymbol{x}, \boldsymbol{x} + \boldsymbol{r}, t) = \big\langle v_{p,i}^{\prime(m)}(t) v_{p,j}^{\prime(n)}(t) \big| \boldsymbol{x} = \boldsymbol{x}_p^{(m)}(t); \boldsymbol{x} + \boldsymbol{r} = \boldsymbol{x}_p^{(n)}(t) \big\rangle. \tag{2.15}$$

The fluid–particle velocity correlation is defined using the fluid fluctuating velocity at the particle centre,

$$R_{ij}^{fp}(\boldsymbol{x}, \boldsymbol{x} + \boldsymbol{r}, t) = \big\langle u_i'(\boldsymbol{x}, t) v_{p,j}^{\prime(n)}(t) \big| \boldsymbol{x} = \boldsymbol{x}_p^{(m)}(t); \boldsymbol{x} + \boldsymbol{r} = \boldsymbol{x}_p^{(n)}(t) \big\rangle, \tag{2.16}$$

$$R_{ij}^{pf}(\boldsymbol{x}, \boldsymbol{x} + \boldsymbol{r}, t) = \big\langle v_{p,i}^{\prime(m)}(t) u_j'(\boldsymbol{x} + \boldsymbol{r}, t) \big| \boldsymbol{x} = \boldsymbol{x}_p^{(m)}(t); \boldsymbol{x} + \boldsymbol{r} = \boldsymbol{x}_p^{(n)}(t) \big\rangle, \tag{2.17}$$

and the fluid–fluid velocity correlation at the particle position,

$$R_{ij}^{ff}(\boldsymbol{x}, \boldsymbol{x} + \boldsymbol{r}, t) = \big\langle u_i'(\boldsymbol{x}, t) u_j'(\boldsymbol{x} + \boldsymbol{r}, t) \big| \boldsymbol{x} = \boldsymbol{x}_p^{(m)}(t); \boldsymbol{x} + \boldsymbol{r} = \boldsymbol{x}_p^{(n)}(t) \big\rangle. \tag{2.18}$$

Note that the correlations given by (2.15) to (2.18) could not be defined for separations smaller than the particle diameter when accounting for inter-particle collision effects because the pair probability for $|\boldsymbol{x} - \boldsymbol{x}^+| < d_p$ is equal to zero. Finally, following Sundaram & Collins (1999), the radial distribution function $g^{pp}(\boldsymbol{x}, \boldsymbol{x} + \boldsymbol{r}, t)$

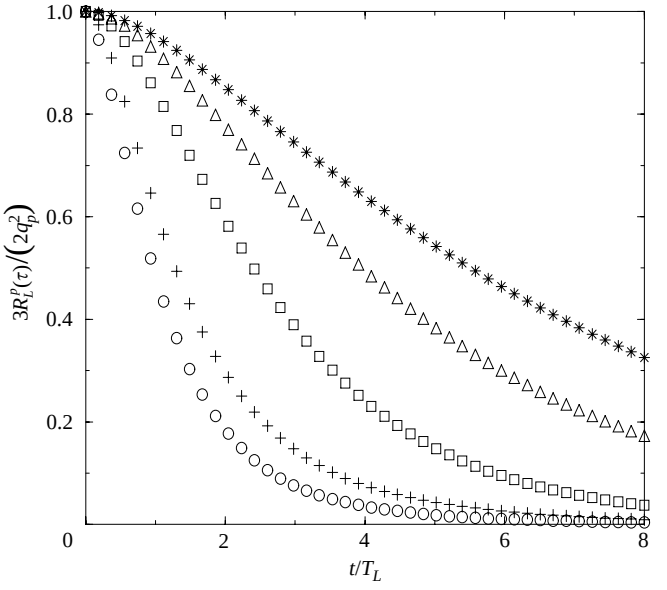

FIGURE 2. Influence of particle inertia on the Lagrangian temporal velocity correlation function $3R_L^p(\tau)/(2q_p^2)$ of finite-inertia particles suspended in isotropic turbulence. The fluid flow is computed using LES at $Re_L = 700$ (see § 4 for details of the computations). Curves correspond to different ratios of the particle relaxation time to fluid Lagrangian integral time scale: ○, $\tau_{fp}^F/T_L = 0.05$; +, $\tau_{fp}^F/T_L = 0.3$; □, $\tau_{fp}^F/T_L = 1.47$; △, $\tau_{fp}^F/T_L = 3.4$; *, $\tau_{fp}^F/T_L = 4.83$.

is introduced, giving the normalized expectation of finding a second particle at a distance $\boldsymbol{r}$ from any given particle,

$$g^{pp}(\boldsymbol{x}, \boldsymbol{x}+\boldsymbol{r}, t) = \frac{\left\langle \delta\left(\boldsymbol{x} - \boldsymbol{x}_p^{(m)}(t)\right)\delta\left(\boldsymbol{x}+\boldsymbol{r} - \boldsymbol{x}_p^{(n)}(t)\right)\right\rangle}{\left\langle \delta\left(\boldsymbol{x} - \boldsymbol{x}_p^{(m)}(t)\right)\right\rangle\left\langle \delta\left(\boldsymbol{x}+\boldsymbol{r} - \boldsymbol{x}_p^{(n)}(t)\right)\right\rangle}. \tag{2.19}$$

In statistically stationary homogeneous turbulence, the above one- and two-point statistics do not depend on spatial coordinates $\boldsymbol{x}$ nor on time t. In addition, in isotropic flow, the two-point velocity correlations can be written in terms of their longitudinal and transverse components, e.g. for the longitudinal particle–particle correlations

$$F^{pp}(r) = \tfrac{1}{3}\left\langle v_{p,i}'^{(m)}(t) v_{p,i}'^{(n)}(t) \middle| \boldsymbol{x} = \boldsymbol{x}_p^{(m)}(t); \boldsymbol{x} + r\boldsymbol{e}_i = \boldsymbol{x}_p^{(n)}(t)\right\rangle, \tag{2.20}$$

with summation over the repeated index i, and where $\boldsymbol{e}_i$ is the unit vector in the i-direction. The transverse correlation is

$$G^{pp}(r) = \tfrac{1}{3}\left\langle v_{p,i}'^{(m)}(t) v_{p,i}'^{(n)}(t) \middle| \boldsymbol{x} = \boldsymbol{x}_p^{(m)}(t); \boldsymbol{x} + r\boldsymbol{e}_j = \boldsymbol{x}_p^{(n)}(t)\right\rangle, \tag{2.21}$$

with $j \neq i$. Analogous expressions may be written for the fluid–particle two-point longitudinal velocity correlations $F^{fp}(r)$ and $F^{pf}(r)$ following (2.16) and (2.17) with $F^{fp}(r) = F^{pf}(r)$ in isotropic turbulence. It is also important to point out that isotropy of the particle fluctuating motion will be assured only when there is no drift between the phases (as would occur with gravitational settling, for example).

2.2. *Lagrangian temporal correlations*

Figure 2 depicts the one-particle Lagrangian temporal correlation of particle velocities normalized by the turbulent kinetic energy of the particulate phase. The Lagrangian

velocity correlations are defined classically along particle trajectories as

$$R_L^p(\tau) = \tfrac{1}{3}\langle v'_{p,i}(t) v'_{p,i}(t+\tau)\rangle_p \tag{2.22}$$

where $\langle\cdot\rangle_p$ is the averaging operator associated with the particle phase, the correlation (2.22) can be computed by averaging over all realizations for any given particle. Figure 2 shows the well-known effect of particles becoming less correlated to their initial velocity with increasing time. The dependence of the Lagrangian velocity correlation on particle inertia is also well known and using the theory of Tchen (1947), the Lagrangian integral time scale, T_L^p, of the particles depends on the particle relaxation time via

$$T_L^p = T_L^{f@p} + \tau_{fp}^F, \tag{2.23}$$

where τ_{fp}^F is defined in § 1.1 and represents the relaxation time averaged over the particles, accounting for nonlinear drag (Simonin 1991), and $T_L^{f@p}$ is the fluid integral time scale sampled along particle trajectories.

For small-inertia particles approaching the scalar limit ($T_L \gg \tau_{fp}^F$), $T_L^{f@p}$ tends to the fluid Lagrangian integral time scale T_L. For large-inertia particles the time scale $T_L^{f@p}$ tends to the fixed-point Eulerian integral time scale of the fluid turbulence T_E (e.g. see Reeks 1977; Pismen & Nir 1978). For intermediate inertia, $T_L^{f@p}$ may be slightly larger than T_L because of the correlation between the particle distribution and regions of the fluid velocity field possessing larger space–time coherence (Février 2000). Typically, the integral time scale T_L^p increases with particle inertia, illustrating the more sluggish change with time of particle velocities, more significant memory of previous motion, and longer times required for adaption of particles to new fluid velocity conditions.

2.3. *Eulerian spatial velocity correlations*

Shown in figure 3 is the longitudinal velocity correlation between two particles at time t, $F^{pp}(r)$, normalized by the particle turbulent kinetic energy q_p^2. For low-inertia particles approaching the scalar limit and adopting the same motion as fluid elements, the longitudinal two-point velocity correlation function $F^{pp}(r)$ of the particle velocities should approach that of the fluid, $F^{ff}(r)$, and should be reasonably well approximated by the exponential $\exp(-r/L_F^f)$ (Hinze 1975) where L_F^f is the longitudinal integral length scale of the fluid turbulence. In the limit r/L_F^f tending to zero, $F^{pp}(r) = F^{ff}(r) \to 2q^2/3$. Note that the condition $r/L_F^f \to 0$ implies that the distance r between the centres of two particles is smaller than any length scale of the fluid turbulence, but larger than the particle diameter. This limit can be defined since the particle diameter is assumed smaller than the Kolmogorov length scale of the turbulent fluid flow. For $r \gg L_F^f$, the two particles under consideration are in fluid velocity regions separated by distances much larger than the integral length scale of the turbulence and therefore the spatial velocity correlation tends to zero. Figure 3 shows that for light particles ($\tau_{fp}^F/T_L = 0.05$ in the figure), the two-point velocity correlations are consistent with the limiting case of fluid elements, i.e. for $r/L_F^f \to 0$, $F^{pp}(r) \to 2q^2/3$. As for the fluid turbulence, when the distance r increases, the particle velocity correlation decreases monotonically. For $r \gg L_F^f$, the spatial velocity correlation is tending towards zero.

For increasing particle inertia, figure 3 shows that the distribution of particle velocities remains spatially correlated, as also shown by Sundaram & Collins (1999) in decaying turbulence, since particles share the same fluid velocity field. Nevertheless,

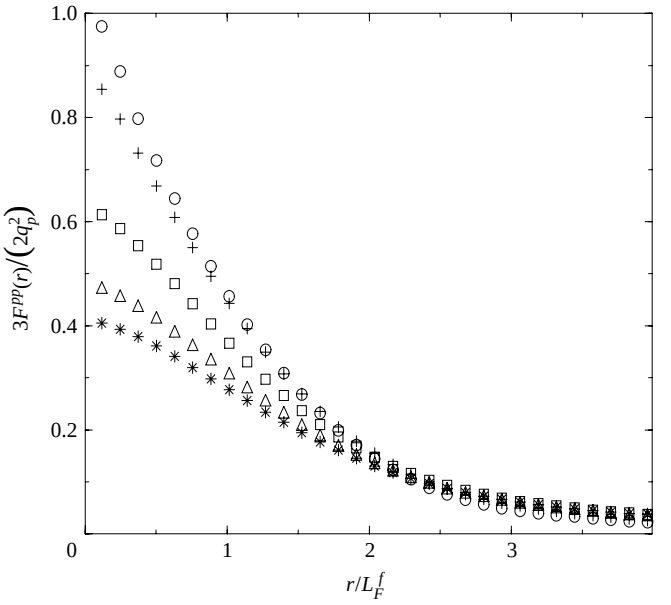

FIGURE 3. Influence of particle inertia on the longitudinal Eulerian spatial correlation function $3F^{pp}(r)/(2q_p^2)$ of finite-inertia particles suspended in isotropic turbulence (same conditions as figure 2).

an important result is that in the limit $r/L_F^f \to 0$, the condition $F^{pp}(r) \to 2q_p^2/3$ is not satisfied, but instead the two-point correlation $F^{pp}(r)$ remains smaller than $2q_p^2/3$.

This feature illustrates that a portion of the particle velocity corresponds to a distribution which is not spatially correlated. Thus, by analogy to the kinetic theory of dilute gases, this contribution is referred to as the quasi-Brownian part of the particle velocity, or quasi-Brownian velocity distribution. Note that if particle motion were completely analogous to molecular motion in a dilute system, the particle positions (in addition to the velocities) would be uncorrelated and the velocity distribution would be Gaussian. For a dilute particle-laden turbulent flow the assumption of molecular chaos implies that the QBVD is not spatially correlated, though there is no requirement *a priori* that the velocity distribution be Gaussian. It is again important to note that the interactions between the particles and fluid turbulent motions which lead to the QBVD are sensitive to particle inertia.

As also shown by figure 3, for increasing inertia, particle velocities may remain correlated even for quite large separations. In contrast, for small separations, the two-particle velocity correlation is decreasing appreciably with increases in particle inertia. This feature illustrates that the quasi-Brownian velocity makes a larger contribution to the particle velocity for increasing response time. Physically, this feature implies that the trajectories of neighbouring particles become independent for very large inertia, approximating the motion of molecules in dilute gases. In this regime, the corresponding particle velocity distribution tends towards Gaussian, consistent with the previous works of Abrahamson (1975) and Reeks (1977).

3. Mesoscopic Eulerian formalism

The aim of this section is to provide a theoretical formalism in order to separately assess the spatially correlated continuous field and the quasi-Brownian distribution of

the particle velocity. The assumption underlying the present formalism is that in dilute two-phase flows any spatial correlation in the dispersed-phase motion is induced via particle interactions with the surrounding fluid motion. Note that this rules out dense regimes, which are not considered, in that interactions between particles (e.g. hydrodynamic effects and inter-particle collisions) may also lead to a spatially correlated particle velocity distribution. Based on the assumption that particle-phase velocity correlations arise due to interactions with the fluid, it is appropriate to develop statistical measures conditioned on a given fluid velocity realization, denoted here as $\mathscr{H}_f$. For the particulate phase this procedure will incorporate information for all scale interactions with the fluid flow and take into account all fluid–particle and particle–particle correlations. A substantial advantage of this approach is that quantities conditioned on the fluid realization $\mathscr{H}_f$ will be local and instantaneous, similar to the instantaneous fluid velocity field.

3.1. *Conditional averaging procedure*

As highlighted in § 1.1 the statistical approach used to analyse the particle velocity – the mesoscopic Eulerian formalism – is based on the presumed chaotic behaviour of inertial particles interacting with a given realization of the gas-phase turbulent flow. One can envision a large number of realizations $\mathscr{H}_p$ of the particulate phase which differ slightly in the initial conditions and yield the same statistics at finite time (for a given fluid flow realization, $\mathscr{H}_f$). Applying the ensemble average over this large number of particulate flow realizations to the refined-grid p.d.f. W_p (cf. § 2.1), the following particle p.d.f. conditioned by the fluid flow realization $\mathscr{H}_f$ can be defined:

$$\widetilde{f}_p^{(1)}(\boldsymbol{x}, \boldsymbol{c}_p, t, \mathscr{H}_f) = \lim_{\mathscr{N}_p \to \infty} \left[\frac{1}{\mathscr{N}_p} \sum_{\mathscr{N}_p} \sum_{m=1}^{N_p} W_p^{(m)}(\boldsymbol{x}, \boldsymbol{c}_p, t, \mathscr{H}_p | \mathscr{H}_f) \right], \tag{3.1}$$

which is the probability of finding a particle at the position $\boldsymbol{x}$ with a velocity $\boldsymbol{c}_p$ at the time t for a given fluid flow realization $\mathscr{H}_f$. The first moment represents the local and instantaneous probable number density of particles,

$$\widetilde{n}_p(\boldsymbol{x}, t, \mathscr{H}_f) = \int \widetilde{f}_p^{(1)}(\boldsymbol{x}, \boldsymbol{c}_p, t, \mathscr{H}_f)\, \mathrm{d}\boldsymbol{c}_p, \tag{3.2}$$

the local and instantaneous velocity of the particles is then

$$\widetilde{v}_{p,i}(\boldsymbol{x}, t, \mathscr{H}_f) = \frac{1}{\widetilde{n}_p(\boldsymbol{x}, t, \mathscr{H}_f)} \int c_{p,i} \widetilde{f}_p^{(1)}(\boldsymbol{x}, \boldsymbol{c}_p, t, \mathscr{H}_f)\, \mathrm{d}\boldsymbol{c}_p. \tag{3.3}$$

The relation (3.3) is referred to as the mesoscopic Eulerian particle velocity field (MEPVF). For a given realization $\mathscr{H}_f$, the velocity $\boldsymbol{v}_p^{(m)}(t)$ of particle m, located at the point $\boldsymbol{x}$ at the time t can be formally written in terms of the instantaneous Eulerian velocity $\widetilde{\boldsymbol{v}}_p(\boldsymbol{x}, t, \mathscr{H}_f)$ and a residual velocity component $\boldsymbol{\delta v}_p^{(m)}(t)$,

$$\boldsymbol{v}_p^{(m)}(t) = \widetilde{\boldsymbol{v}}_p\left(\boldsymbol{x}_p^{(m)}(t), t, \mathscr{H}_f\right) + \boldsymbol{\delta v}_p^{(m)}(t). \tag{3.4}$$

It should be emphasized that the MEPVF is defined in the Eulerian frame of reference and therefore can be considered as a velocity field shared by all particles of the system. In contrast, the particle velocity $\boldsymbol{v}_p$, as well as the residual component $\boldsymbol{\delta v}_p$, are Lagrangian quantities associated with individual particles and defined along trajectories. This dependence is stressed by the superscript (m) which identifies a given particle. As will be shown in § 3.3, the decomposition of the particle velocity given by relation (3.4) is unique, splitting the particle velocity into contributions that take into

account the spatial structure (correlation) of the velocity field in the first term and spatially uncorrelated motion in the second term.

Using the properties of the statistical operator $\langle\cdot\rangle$, the residual velocity $\boldsymbol{\delta v}_p(t)$ satisfies the relation

$$\langle \boldsymbol{\delta v}_p(t) | \boldsymbol{x} = \boldsymbol{x}_p(t); \mathscr{H}_f \rangle = 0. \tag{3.5}$$

Important properties derived from the residual velocity $\boldsymbol{\delta v}_p(t)$ include the kinetic stress,

$$\delta\widetilde{\sigma}_{p,ij}(\boldsymbol{x}, t, \mathscr{H}_f) = \langle \delta v_{p,i} \delta v_{p,j} | \boldsymbol{x}_p(t) = \boldsymbol{x}; \mathscr{H}_f \rangle, \tag{3.6}$$

and quasi-Brownian kinetic energy,

$$\delta\widetilde{\theta}_p(\boldsymbol{x}, t, \mathscr{H}_f) = \tfrac{1}{2}\delta\widetilde{\sigma}_{p,ii} = \langle \delta v_{p,i} \delta v_{p,i} | \boldsymbol{x}_p(t) = \boldsymbol{x}; \mathscr{H}_f \rangle. \tag{3.7}$$

3.2. *Macroscopic quantities related to the MEPVF*

The mesoscopic Eulerian velocity field of the particulate phase as developed above can be considered similar to a compressible fluid with density $\widetilde{n}_p(\boldsymbol{x}, t, \mathscr{H}_f)$ and velocity $\widetilde{\boldsymbol{v}}_p(\boldsymbol{x}, t, \mathscr{H}_f)$. Macroscopic quantities can be derived by applying a density-weighted average, similar to Favre averaging in compressible gases, but in this case using the particle number density. The averaging is carried out over a large number of realizations of the mesoscopic Eulerian field, i.e. over a large number of fluid flow realizations $\mathscr{H}_f$. Consequently, one- and two-point statistics formed using $\widetilde{n}_p$ and $\widetilde{\boldsymbol{v}}_p$ may be defined. Furthermore, noting that $\langle\cdot\rangle = \langle\langle\cdot|\mathscr{H}_f\rangle\rangle$, theoretical relations between these macroscopic quantities can be derived and some of them are presented in the following section. Further details are given in the Appendix.

3.2.1. *One-point statistics of the MEPVF*

The mean velocity of the MEPVF is defined as

$$\widetilde{\boldsymbol{V}}_p(\boldsymbol{x}, t) = \frac{\langle \widetilde{n}_p(\boldsymbol{x}, t, \mathscr{H}_f) \widetilde{\boldsymbol{v}}_p(\boldsymbol{x}, t, \mathscr{H}_f) \rangle}{\langle \widetilde{n}_p(\boldsymbol{x}, t, \mathscr{H}_f) \rangle} = \langle \widetilde{\boldsymbol{v}}_p \rangle_p, \tag{3.8}$$

and is identical to the mean velocity of the particulate phase, i.e. $\widetilde{\boldsymbol{V}}_p = \boldsymbol{V}_p$ (cf. (2.3)). Note also the notation in the last term in (3.8), $\langle\cdot\rangle_p$, which is used to more compactly indicate the number density-weighted average. In addition, $\langle \widetilde{n}_p(\boldsymbol{x}, t, \mathscr{H}_f) \rangle = n_p(\boldsymbol{x}, t)$ (cf. (2.2)). The mean kinetic energy of the fluctuating (or turbulent) part of the MEPVF is defined as

$$\widetilde{q}_p^2(\boldsymbol{x}, t) = \frac{1}{2} \frac{\langle \widetilde{n}_p(\boldsymbol{x}, t, \mathscr{H}_f) \widetilde{v}'_{p,i}(\boldsymbol{x}, t, \mathscr{H}_f) \widetilde{v}'_{p,i}(\boldsymbol{x}, t, \mathscr{H}_f) \rangle}{\langle \widetilde{n}_p(\boldsymbol{x}, t, \mathscr{H}_f) \rangle} = \frac{1}{2} \langle \widetilde{v}'_{p,i} \widetilde{v}'_{p,i} \rangle_p, \tag{3.9}$$

where $\widetilde{\boldsymbol{v}}'_p(\boldsymbol{x}, t, \mathscr{H}_f) = \widetilde{\boldsymbol{v}}_p(\boldsymbol{x}, t, \mathscr{H}_f) - \langle \widetilde{\boldsymbol{v}}_p \rangle_p(\boldsymbol{x}, t)$ is the fluctuating velocity of the instantaneous Eulerian particulate velocity. The component $\widetilde{q}_p^2$ is related to the total turbulent kinetic energy q_p^2 through the relation

$$\widetilde{q}_p^2 + \delta q_p^2 = q_p^2. \tag{3.10}$$

This relation simply represents the total fluctuating kinetic energy in terms of the sum of the contribution from $\widetilde{\boldsymbol{v}}_p$ and the mean kinetic energy δq_p^2 of the residual velocity distribution $\boldsymbol{\delta v}_p$,

$$\delta q_p^2(\boldsymbol{x}, t) = \frac{\langle \widetilde{n}_p(\boldsymbol{x}, t, \mathscr{H}_f) \delta\widetilde{\theta}_p(\boldsymbol{x}, t, \mathscr{H}_f) \rangle}{\langle \widetilde{n}_p(\boldsymbol{x}, t, \mathscr{H}_f) \rangle} = \langle \delta\widetilde{\theta}_p \rangle_p. \tag{3.11}$$

The fluid–particle Eulerian velocity covariance is defined as

$$\widetilde{q}_{fp}(\boldsymbol{x},t)=\frac{\langle\widetilde{n}_p(\boldsymbol{x},t,\mathscr{H}_f)u_i'(\boldsymbol{x},t)\widetilde{v}_{p,i}'(\boldsymbol{x},t,\mathscr{H}_f)\rangle}{\langle\widetilde{n}_p(\boldsymbol{x},t,\mathscr{H}_f)\rangle}=\langle u_i'\widetilde{v}_{p,i}'\rangle_p. \tag{3.12}$$

As shown in the Appendix, the residual velocity $\boldsymbol{\delta v}_p$ of any particle is not correlated with the undisturbed fluid velocity at the location of the particle centre,

$$\langle u_i'(x,t)\delta v_{p,j}(t)|\boldsymbol{x}=\boldsymbol{x}_p(t)\rangle=0, \tag{3.13}$$

for all i and j. Consequently, the Eulerian fluid–particle velocity covariance $\widetilde{q}_{fp}$ and the total fluid–particle velocity covariance q_{fp} are identical, i.e. $\widetilde{q}_{fp}=q_{fp}$. Therefore, the MEPVF completely accounts for all one-point fluid–particle velocity correlations. Finally, the fluid turbulence kinetic energy sampled along particle trajectories is defined as

$$\widetilde{q}^2_{f@p}(\boldsymbol{x},t)=\frac{1}{2}\frac{\langle\widetilde{n}_p(\boldsymbol{x},t,\mathscr{H}_f)u_i'(\boldsymbol{x},t)u_i'(\boldsymbol{x},t)\rangle}{\langle\widetilde{n}_p(\boldsymbol{x},t,\mathscr{H}_f)\rangle}=\frac{1}{2}\langle u_i'u_i'\rangle_p, \tag{3.14}$$

and the development in the Appendix shows $\widetilde{q}^2_{f@p}=q^2_{f@p}$.

3.2.2. *Two-point statistics of the MEPVF*

As already shown, the mesoscopic Eulerian quantities $\widetilde{n}_p$ and $\widetilde{\boldsymbol{v}}_p'$ are functions of the fluid realization $\mathscr{H}_f$. For the sake of more compact notation in the following, this dependence is not explicitly indicated in the development of the two-point relations presented in this section. The macroscopic two-point correlations defined in terms of the MEPVF are derived via averaging over a large number of fluid flow realizations and therefore these quantities are not functions of $\mathscr{H}_f$.

Sundaram & Collins (1997) accounted for the influence of the spatial distribution of the particulate phase on collision rates by introducing the radial distribution function at contact. The radial distribution function $\widetilde{g}^{pp}$ defined in terms of the MEPVF is

$$\widetilde{g}^{pp}(\boldsymbol{x},\boldsymbol{x}+\boldsymbol{r},t)=\frac{\langle\widetilde{n}_p(\boldsymbol{x},t,\mathscr{H}_f)\widetilde{n}_p(\boldsymbol{x}+\boldsymbol{r},t,\mathscr{H}_f)\rangle}{\langle\widetilde{n}_p(\boldsymbol{x},t,\mathscr{H}_f)\rangle\,\langle\widetilde{n}_p(\boldsymbol{x}+\boldsymbol{r},t,\mathscr{H}_f)\rangle}. \tag{3.15}$$

The particle–particle velocity correlations is

$$\widetilde{R}^{pp}_{ij}(\boldsymbol{x},\boldsymbol{x}+\boldsymbol{r},t)=\frac{\langle\widetilde{n}_p(\boldsymbol{x},t)\widetilde{v}_{p,i}'(\boldsymbol{x},t)\widetilde{n}_p(\boldsymbol{x}+\boldsymbol{r},t)\widetilde{v}_{p,j}'(\boldsymbol{x}+\boldsymbol{r},t)\rangle}{\langle\widetilde{n}_p(\boldsymbol{x},t)\widetilde{n}_p(\boldsymbol{x}+\boldsymbol{r},t)\rangle}, \tag{3.16}$$

the fluid–particle velocity correlations are

$$\widetilde{R}^{fp}_{ij}(\boldsymbol{x},\boldsymbol{x}+\boldsymbol{r},t)=\frac{\langle\widetilde{n}_p(\boldsymbol{x},t)u_i'(\boldsymbol{x},t)\widetilde{n}_p(\boldsymbol{x}+\boldsymbol{r},t,)\widetilde{v}_{p,j}'(\boldsymbol{x}+\boldsymbol{r},t)\rangle}{\langle\widetilde{n}_p(\boldsymbol{x},t)\widetilde{n}_p(\boldsymbol{x}+\boldsymbol{r},t)\rangle}, \tag{3.17}$$

$$\widetilde{R}^{pf}_{ij}(\boldsymbol{x},\boldsymbol{x}+\boldsymbol{r},t)=\frac{\langle\widetilde{n}_p(\boldsymbol{x},t)\widetilde{v}_{p,i}'(\boldsymbol{x},t)\widetilde{n}_p(\boldsymbol{x}+\boldsymbol{r},t)u_j'(\boldsymbol{x}+\boldsymbol{r},t)\rangle}{\langle\widetilde{n}_p(\boldsymbol{x},t)\widetilde{n}_p(\boldsymbol{x}+\boldsymbol{r},t)\rangle}, \tag{3.18}$$

and the fluid–fluid velocity correlation at the particle position is

$$\widetilde{R}^{ff}_{ij}(\boldsymbol{x},\boldsymbol{x}+\boldsymbol{r},t)=\frac{\langle\widetilde{n}_p(\boldsymbol{x},t)u_i'(\boldsymbol{x},t)\widetilde{n}_p(\boldsymbol{x}+\boldsymbol{r},t)u_j'(\boldsymbol{x}+\boldsymbol{r},t)\rangle}{\langle\widetilde{n}_p(\boldsymbol{x},t)\widetilde{n}_p(\boldsymbol{x}+\boldsymbol{r},t)\rangle}. \tag{3.19}$$

3.3. *Theoretical relations in dilute turbulent two-phase flow*

The two-point correlations of the particle velocity (see § 2.3) highlight the two contributions to the translation velocity of any particle: a spatially correlated component

and a 'quasi-Brownian' velocity not correlated in space (and therefore not continuous). The MEF provides an approach that expresses the particle velocity in terms of a local-instantaneous Eulerian field $\widetilde{\boldsymbol{v}}_p(\boldsymbol{x}, t, \mathscr{H}_f)$ and a residual component $\boldsymbol{\delta v}_p(t)$. The developments in the previous section (and also summarized more completely in the Appendix) show that the velocity field $\widetilde{\boldsymbol{v}}_p(\boldsymbol{x}, t)$ completely accounts for the one-point fluid–particle velocity correlations since the residual velocity $\boldsymbol{\delta v}_p(t)$ of any particle is not correlated to the fluid velocity measured at the particle centre. Therefore, it seems legitimate to expect that the residual velocities $\boldsymbol{\delta v}_p(t)$ comprise the quasi-Brownian distribution of the particulate phase. That correspondence is made definitive in this section.

Considering any two particles m and n ($m \neq n$) of the system, for a given fluid flow realization, the two-particle pair distribution function $\widetilde{f}_p^{(2)}$ is defined,

$$\widetilde{f}_p^{(2)}(\boldsymbol{x}, \boldsymbol{c}_p, \boldsymbol{x}^+, \boldsymbol{c}_p^+, t, \mathscr{H}_f) = \lim_{\mathscr{N}_p \to \infty} \left[\frac{1}{\mathscr{N}_p} \sum_{\mathscr{N}_p} \sum_{m=1}^{N_p} \sum_{n=1}^{N_p} W_p^{(m,n)}(\boldsymbol{x}, \boldsymbol{c}_p, \boldsymbol{x}^+, \boldsymbol{c}_p^+, t, \mathscr{H}_p | \mathscr{H}_f) \right]. \tag{3.20}$$

For the gas–solid flows under consideration – dilute regimes for which turbulence modulation and inter-particle interactions (hydrodynamic interactions and inter-particle collisions) are neglected – the trajectory of any particle is fully defined by its initial conditions and via interactions with the fluid velocity field. Because of the presumed chaotic nature of the particle motion as discussed § 3.1, trajectories become independent of initial conditions and, consequently, are fully defined by the fluid flow realization. This implies that trajectories of two particles will be dependent only through interactions with a shared fluid velocity field. Therefore, by considering any two particles m and n ($m \neq n$), the $\mathscr{H}_f$-conditioned probability of finding a particle m at a point $\boldsymbol{x}$ with a velocity $\boldsymbol{c}_p$ is independent of the position and velocity of the other particle n. This independence allows the two-particle p.d.f. to be expressed in terms of the one-particle p.d.f.s,

$$\widetilde{f}_p^{(2)}(\boldsymbol{x}, \boldsymbol{c}_p, \boldsymbol{x}^+, \boldsymbol{c}_p^+, t, \mathscr{H}_f) = \frac{N_p(N_p - 1)}{{N_p}^2} \widetilde{f}_p^{(1)}(\boldsymbol{x}, \boldsymbol{c}_p, t, \mathscr{H}_f) \widetilde{f}_p^{(1)}(\boldsymbol{x}^+, \boldsymbol{c}_p^+, t, \mathscr{H}_f). \tag{3.21}$$

Relation (3.21) therefore shows that the probability distribution function $\widetilde{f}_p^{(1)}$ provides a complete description of the spatially correlated motion of the particulate phase. Some of the important properties developed from (3.21) (and more completely developed in the Appendix) are:

1. The velocity $\boldsymbol{\delta v}_p$ is not spatially correlated with the instantaneous fluid velocity field, i.e., $\langle u_i'(\boldsymbol{x}, t) \delta v_{p,j}^{(n)}(t) | \boldsymbol{x} + \boldsymbol{r} = \boldsymbol{x}_p^{(n)}(t) \rangle = 0$. More specifically, $\boldsymbol{\delta v}_p$ is not spatially correlated to the instantaneous locally-undisturbed fluid velocity at the position of any particle, $\langle u_i'(\boldsymbol{x}, t) \delta v_{p,j}^{(n)}(t) | \boldsymbol{x} = \boldsymbol{x}_p^{(m)}(t); \boldsymbol{x} + \boldsymbol{r} = \boldsymbol{x}_p^{(n)}(t) \rangle = 0$.

2. The component $\boldsymbol{\delta v}_p$ is not spatially correlated to the instantaneous Eulerian velocity field $\widetilde{\boldsymbol{v}}_p$, i.e. $\langle \widetilde{v}_{p,i}'(\boldsymbol{x}, t) \delta v_{p,j}^{(n)}(t) | \boldsymbol{x} = \boldsymbol{x}_p^{(m)}(t); \boldsymbol{x} + \boldsymbol{r} = \boldsymbol{x}_p^{(n)}(t) \rangle = 0$.

3. The velocities $\boldsymbol{\delta v}_p$ of any two ($m \neq n$) particles are not correlated, $\langle \delta v_{p,j}^{(m)}(t) \, \delta v_{p,j}^{(n)}(t) | \boldsymbol{x} = \boldsymbol{x}_p^{(m)}(t); \boldsymbol{x} + \boldsymbol{r} = \boldsymbol{x}_p^{(n)}(t) \rangle = 0$.

The relation (3.21) and properties summarized above which follow are important results since they show that the decomposition of the particle velocity (3.4) is unique – the residual component $\boldsymbol{\delta v}_p$ is precisely the quasi-Brownian velocity of the particle. Using other decompositions, e.g. as commonly considered when time- or

volume-averaging the equations of motion, similar interpretations are not possible. Furthermore, all of the information concerning the spatial structure of the particle velocity field and its correlation with the fluid flow is accounted for in the MEPVF, and for $r \geqslant d_p$,

$$g^{pp}(\boldsymbol{x}, \boldsymbol{x}+\boldsymbol{r}, t) = \widetilde{g}^{pp}(\boldsymbol{x}, \boldsymbol{x}+\boldsymbol{r}, t), \tag{3.22}$$

$$R_{ij}^{pp}(\boldsymbol{x}, \boldsymbol{x}+\boldsymbol{r}, t) = \widetilde{R}_{ij}^{pp}(\boldsymbol{x}, \boldsymbol{x}+\boldsymbol{r}, t), \tag{3.23}$$

$$R_{ij}^{fp}(\boldsymbol{x}, \boldsymbol{x}+\boldsymbol{r}, t) = \widetilde{R}_{ij}^{fp}(\boldsymbol{x}, \boldsymbol{x}+\boldsymbol{r}, t), \tag{3.24}$$

$$R_{ij}^{ff}(\boldsymbol{x}, \boldsymbol{x}+\boldsymbol{r}, t) = \widetilde{R}_{ij}^{ff}(\boldsymbol{x}, \boldsymbol{x}+\boldsymbol{r}, t). \tag{3.25}$$

It should be noted that the correlations derived from the MEPVF, e.g. $\widetilde{R}_{ij}^{pp}$, are well-defined for a continuum, i.e. for $r < d_p$, while the two-point velocity correlations R_{ij}^{pp} are theoretically defined for any two particles separated by a distance larger than d_p.

Finally, (3.21) should also be valid in dilute systems even when inter-particle collisions are taken into account. By analogy with the kinetic theory of dilute gases, the trajectories of particles in the limiting regime of molecular chaos can be assumed independent, except during a collision event. Making a similar assumption for other regimes in dilute gas–solid flows leads to the conclusion that inter-particle collisions will not induce spatial correlations in the particle velocity field and that (3.21) is valid for $|x - x^+| > d_p$.

Part II. Numerical study of the particle velocity field in isotropic turbulence

In this section numerical simulation of isotropic turbulence laden with small heavy particles is used to study the spatial characteristics of turbulent gas–solid flows. Direct numerical simulation (DNS) of the fluid turbulence along with discrete particle tracking for the dispersed phase is employed, an approach that has been widely used in several previous studies (e.g. see Squires & Eaton 1991*a*, *b*; Elghobashi & Truesdell 1993; Wang & Maxey 1993; Sundaram & Collins 1997; Wang *et al.* 2000; Reade & Collins 2000). Though DNS remains the most satisfactory approach from a theoretical point of view, it is limited to moderate Reynolds numbers, constraining particle parameters that may be realistically considered.

An alternative technique that is less constrained and therefore also employed in the present study is large-eddy simulation (LES) – direct resolution of the large turbulent scales of the flow, with empiricism used to parameterize the effect of the small subgrid scales of motion on the large eddies. LES is a useful approach for gas–solid flows since the filtering effect of particle inertia results in relatively small errors in particle-phase statistics due to the fact that the high-frequency gas-phase velocity fluctuations are not directly resolved. The influence of the subgrid motions on particle transport further decreases with increasing particle response times compared to the time scales of the subgrid motions (e.g. see Yeh & Lei 1991; Deutsch & Simonin 1991; Simonin, Deutsch & Boivin 1995; Wang & Squires 1996; Boivin, Simonin & Squires 2000; Février 2000; Yamamoto *et al.* 2001). Important to note, however, is that the filtering of small subgrid-scale fluid velocity fluctuations is only effective when the particle response time is sufficiently large compared to the smallest resolved time scales of the LES. While these and other studies have shown that statistical features dominated by the large scales, including quantities such as turbulent dispersion and the particulate-phase kinetic energy, can be accurately recovered using LES, of particular interest to

the present simulations is application of LES for prediction of spatial structure, i.e. the two-point velocity correlations.

Particle concentrations in the two-phase flows considered in the computations are dilute, the influence of fluid turbulence modulation by the particle is neglected, as are influences of inter-particle interactions. The particular flow under consideration is statistically stationary isotropic turbulence with a dispersed phase of heavy particles whose motion is governed by drag and without the effect of any body forces such as gravity. Although perhaps the most canonical three-dimensional turbulent flow, fluid turbulence dynamics and particle motion are complex and not easily predicted. The configuration considered here also possesses the advantage that the particulate phase attains a dynamical equilibrium with the fluid flow, enabling a verification of many of the statistical features of particle motion against theoretical relations.

To assess the spatial features of the particulate phase, the MEF is applied in an *a priori* fashion to the results of the Euler–Lagrange simulation. The computational burden imposed for accurate analysis using the MEF is significant, requiring a large number of particle-system realizations for a single fluid flow realization and § 5 is devoted to a summary of the tests used to assess the accuracy of the numerical procedures. Following the validation, the primary aim is to use of the results from the Euler–Lagrange simulation to calculate the MEPVF (a property of all the particles) and the QBVD (for each particle). Taking advantage of the homogeneity and ergodicity of the two-phase flow, space and time averaging is performed to assess the macroscopic statistical quantities of the particle phase, using both single-point and two-point measures. The results are compared to the theoretical predictions obtained from the MEF and also used to investigate the effect of particle inertia on the spatial features of the gas–solid flow.

4. Simulation overview

4.1. *Fluid phase*

The three-dimensional time-dependent incompressible Navier–Stokes equations are solved on a triply periodic cubic domain. The equations are integrated on a staggered grid using centred second-order-accurate spatial differences. The discretized equations are time advanced using a second-order Runge–Kutta scheme. In the large-eddy simulations, the dynamic mixed model of Zang, Street & Koseff (1993) is used to close the subgrid-scale stress. The formulation and its implementation in the current solver is the same as described in Calmet & Magnaudet (1997). The flows are made statistically stationary by forcing the low-wavenumber components of the velocity field. The particular method is that developed by Eswaran & Pope (1988). The forcing is accomplished by means of a complex vector-valued Uhlenbeck–Ornstein stochastic process. All wavenumbers between two spherical shells of radius κ_{Fmin} and κ_{Fmax} are subjected to forcing. Yeung & Pope (1989) showed that forcing the wavenumber range $]0;2\sqrt{2}\kappa_0]$ (where κ_0 is the lowest non-zero wavenumber) can lead to overly large influences of the periodic boundary conditions employed in the calculations on the resulting turbulent flow. Thus, for the primary computations reported in this work the forced modes were in the range $\kappa_{Fmin} = 2\kappa_0$ and $\kappa_{Fmax} = 6\kappa_0$. These values represent a compromise between contamination of flow-field statistics due to artifacts of the forcing scheme and the boundary conditions (Février 2000). The correlation time scale associated with the forcing scheme is chosen to ensure $T_E \approx T_e$, where T_e is the eddy-turnover time defined as $T_e = L_F^f/u'$. Note that the Eulerian integral time scale denoted T_E is defined from the temporal velocity correlation sampled at fixed

	$[\kappa_{Fmin};\kappa_{Fmax}]$	Re_L	$Re_{\lambda_G^f}$	u'	ϵ	L_F^f	T_L	T_L/τ_η	$\kappa_{max}\eta$
DNS 128^3	$[2\kappa_0;6\kappa_0]$	110	52	0.160	0.236	0.0104	0.051	6.40	1.086
LES 96^3	$[2\kappa_0;6\kappa_0]$	700	134	0.145	0.188	0.0096	0.054	16.6	0.190
DNS 96^3	$]0;2\sqrt{2}\kappa_0]$	140	67	0.126	0.053	0.0166	0.130	7.73	1.183

TABLE 1. Fluid flow simulation parameters.

points,

$$T_E = \int \frac{1}{2}\frac{\langle u_i'(x,t)u_i'(x,t+\tau)\rangle}{q^2}\,\mathrm{d}\tau. \tag{4.1}$$

Summarized in table 1 are parameters of the fluid flow after the simulations have evolved to a statistically stationary condition. The parameters in table 1 are the turbulent Reynolds number $Re_L = L_F^f u'/\nu$ (where ν is the kinematic viscosity), the Taylor-microscale Reynolds number $Re_{\lambda_G^f} = \lambda_G^f u'/\nu$ (where λ_G^f is the transverse Taylor microscale), the r.m.s. fluid fluctuating velocity component $u' = (2q^2/3)^{1/2}$ (where q^2 is the fluid turbulent kinetic energy), the energy dissipation rate ϵ, the integral length scale of the longitudinal spatial velocity correlation L_F^f, and the Lagrangian integral time scale T_L. The Kolmogorov length scale $\eta = (\nu^3/\epsilon)^{1/4}$ and time scale $\tau_\eta = (\nu/\epsilon)^{1/2}$ are also tabulated. Three computations of the fluid turbulence are reported, a 128^3 DNS at $Re_L = 110$ and a 96^3 LES at $Re_L = 700$, both with forcing applied on the wavenumber range $[2\kappa_0;6\kappa_0]$. A 96^3 DNS at $Re_L = 140$ with forcing on the range $]0;2\sqrt{2}\kappa_0]$ was also performed. The 96^3 DNS introduces more variability in the flow-field statistics via the change in forced modes, in turn providing some insight into the effects of the forcing on properties of the two-phase flow. Values of the parameter $\kappa_{max}\eta$ (where κ_{max} is the highest resolvable wavenumber) are also summarized in the table. As shown, for the DNS the values are larger than unity, consistent with previous work that indicates that $\kappa_{max}\eta > 1$ is adequate for resolution of small-scale features (e.g. see Yeung & Pope 1989 and Balachandar & Maxey 1989).

4.2. *Particulate-phase treatment*

The particulate phase is composed of a mono-disperse mixture of particles with diameters d_p smaller than the Kolmogorov length scale. Gas–solid mixtures are considered in which the particle density is large compared to the fluid value ($O(1000)$). In this regime, particle motion is governed mainly by drag, and the equation of motion used to determine the velocity of the particles takes the form

$$\frac{\mathrm{d}\boldsymbol{x}_p}{\mathrm{d}t} = \boldsymbol{v}_p, \qquad \frac{\mathrm{d}\boldsymbol{v}_p}{\mathrm{d}t} = \frac{\rho}{\rho_p}\frac{18\nu}{d_p^2}(\boldsymbol{u}-\boldsymbol{v}_p)f_D, \tag{4.2}$$

where $\boldsymbol{v}_p$ and $\boldsymbol{x}_p$ are the velocity and the centre position of a particle, and $\boldsymbol{u}$ is the value of the fluid velocity undisturbed by the presence of the particle at the particle centre. For the computations performed in this study, the particle Reynolds number, $Re_p = d_p|\boldsymbol{u}-\boldsymbol{v}_p|/\nu$ is less than 10. As is appropriate for this regime, the drag force is modified using the empirical relation of Schiller & Nauman (1935),

$$f_D = 1 + 0.15Re_p^{0.687}. \tag{4.3}$$

For the current simulations in which turbulence modulation by particles is neglected, the undisturbed value is the fluid velocity resolved by the DNS and LES. In the LES this fluid velocity represents the spatially filtered (volume averaged) solution of the

Navier–Stokes equations. The influence of subgrid-scale transport on particle motion is not considered, which is a reasonable assumption so long as the particle response time is sufficiently large compared to the smallest resolved time scales of the LES in order that subgrid velocity fluctuations will be effectively filtered by particle inertia.

For a single calculation of the fluid flow, simultaneous computation of several particle classes were performed, with each class corresponding to a particular set of particle parameters. Particle Stokes numbers were calculated at the conclusion of a simulation, using the fluid Lagrangian time scale T_L and averaged particle time constant, $St = \tau_{fp}^F / T_L$. The mean particle relaxation time is defined as

$$\tau_{fp}^F = \frac{d_p^2}{18\nu} \frac{\rho_p}{\rho} \frac{1}{\langle f_D \rangle}, \tag{4.4}$$

where the average is taken with respect to the dispersed phase. A reasonably wide distribution in time constants was considered in order to investigate the particulate-phase properties ranging from very low-inertia particles capable of nearly following the motion of fluid elements to very large-inertia particles that were quite unresponsive to the spectrum of fluid turbulent motions. The resulting Stokes numbers range from $St = 0.02$ to $St = 10$ for the simulations presented in this manuscript.

Particles are introduced into the computational domain at random initial positions with zero initial velocity. In agreement with Wang & Maxey (1993), the transient prior to the equilibration of the r.m.s. particle velocity is about $3\tau_{fp}^F$, while it is about $2T_e$ for the concentration distribution. Statistics are acquired over at least $12T_e$, after the two-phase flow has reached statistical equilibrium. Particle sample sizes in the computations were varied from 3×10^5 to 10×10^6. The largest sample sizes were used in calculations to extract detailed information concerning properties of the MEPVF and QBVD. As also described below, statistical features could be accurately acquired using smaller sample sizes, and the adequacy of the sample, and of the approach in general, is verified using the theoretical relations developed in Part I above. In the following, statistical features normalized by large-scale variables are considered. Such normalization is adequate for long-time statistics such as the kinetic energy and turbulent dispersion since these quantities are governed by the interaction of particles with the large scales of the turbulence (e.g. see Hinze 1975). This normalization is shown to be adequate for analysis of the long-time statistics of the MEPVF and QBVD.

4.3. *Approximation of the MEPVF*

The MEF is based on ensemble averaging over a large number of realizations of the particulate-phase system, conditioned on a single fluid flow realization. The evaluation of the MEF using the simulation database is performed using local volume averages. This requires sufficient particle sample sizes within any volume in order to obtain meaningful statistics and also that the volume dimensions be sufficiently small such that there is effectively no variation in the mesoscopic field of the particles. Provided these criteria are satisfied, these two procedures – ensemble averaging and volume averaging – will yield the same statistics.

The MEPVF is resolved over small volumes $\Omega = (\Delta y)^3$ in which the length scale Δy is equal to or smaller than the corresponding grid spacing used for resolution of the fluid flow, i.e. $\Delta y \leqslant \Delta x$. The instantaneous Eulerian properties of the particulate

phase expressed in terms of the local volume averages take the form

$$\widetilde{n}_p(\boldsymbol{x}, t, \mathscr{H}_f) \equiv \frac{1}{\Omega(\boldsymbol{x})} \int_{\Omega(\boldsymbol{X})} \left\langle \sum_{m=1}^{N_p} \delta\big(\boldsymbol{r} - \boldsymbol{x}_p^{(m)}(t)\big) | \mathscr{H}_f \right\rangle \mathrm{d}\boldsymbol{r}, \tag{4.5}$$

$$\widetilde{\boldsymbol{v}}_p(\boldsymbol{x}, t, \mathscr{H}_f) \equiv \frac{1}{\Omega(\boldsymbol{x})} \int_{\Omega(\boldsymbol{X})} \frac{\left\langle \sum_{m=1}^{N_p} \boldsymbol{v}_p^{(m)}(t) \delta\big(\boldsymbol{r} - \boldsymbol{x}_p^{(m)}(t)\big) | \mathscr{H}_f \right\rangle}{\left\langle \sum_{m=1}^{N_p} \delta\big(\boldsymbol{r} - \boldsymbol{x}_p^{(m)}(t)\big) | \mathscr{H}_f \right\rangle} \mathrm{d}\boldsymbol{r}, \tag{4.6}$$

$$\boldsymbol{u}(\boldsymbol{x}, t) \equiv \frac{1}{\Omega(\boldsymbol{x})} \int_{\Omega(\boldsymbol{X})} \frac{\left\langle \sum_{m=1}^{N_p} \boldsymbol{u}(\boldsymbol{r}, t) \delta\big(\boldsymbol{r} - \boldsymbol{x}_p^{(m)}(t)\big) | \mathscr{H}_f \right\rangle}{\left\langle \sum_{m=1}^{N_p} \delta\big(\boldsymbol{r} - \boldsymbol{x}_p^{(m)}(t)\big) | \mathscr{H}_f \right\rangle} \mathrm{d}\boldsymbol{r}. \tag{4.7}$$

For the applications considered in this study, the bin volumes Ω are cubic, consistent with the orthogonal mesh used for resolution of the Navier–Stokes equations, and in the following the volume dimension Δy is varied in order to assess the sensitivity of the MEPVF to Δy and to determine a practical value for subsequent computations.

4.4. *Numerical approach for the evaluation of the MEPVF*

From a practical standpoint, it is preferable to calculate the MEPVF by first integrating the particle velocity over volume Ω, and then by averaging over a large number of realizations of the particle-phase system. Interchange of the operations of integration and averaging yields an expression for the local number density,

$$\widetilde{n}_p(\boldsymbol{x}, t, \mathscr{H}_f) = \left\langle \left[\frac{1}{\Omega(\boldsymbol{x})} \int_{\Omega(\boldsymbol{X})} \sum_{m=1}^{N_p} \delta\big(\boldsymbol{r} - \boldsymbol{x}_p^{(m)}(t)\big) \, \mathrm{d}\boldsymbol{r} \right] \middle| \, \mathscr{H}_f \right\rangle. \tag{4.8}$$

Assuming the variation of the local particle number density $\widetilde{n}_p$ is small within the volume $\Omega(\boldsymbol{x})$, it is possible to approximate (4.6) as

$$\widetilde{\boldsymbol{v}}_p(\boldsymbol{x}, t, \mathscr{H}_f) \approx \frac{1}{\widetilde{n}_p(\boldsymbol{x}, t, \mathscr{H}_f)} \left\langle \left[\frac{1}{\Omega(\boldsymbol{x})} \int_{\Omega(\boldsymbol{X})} \sum_{m=1}^{N_p} \boldsymbol{v}_p^{(m)}(t) \delta\big(\boldsymbol{r} - \boldsymbol{x}_p^{(m)}(t)\big) \mathrm{d}\boldsymbol{r} \right] \middle| \, \mathscr{H}_f \right\rangle. \tag{4.9}$$

The instantaneous fluid velocity along the particle trajectory is approximated in the same manner,

$$\boldsymbol{u}(\boldsymbol{x}, t) \approx \frac{1}{\widetilde{n}_p(\boldsymbol{x}, t)} \left\langle \left[\frac{1}{\Omega(\boldsymbol{x})} \int_{\Omega(\boldsymbol{X})} \sum_{m=1}^{N_p} \boldsymbol{u}(\boldsymbol{r}, t) \delta(\boldsymbol{r} - \boldsymbol{x}_p^{(m)}(t)) \, \mathrm{d}\boldsymbol{r} \right] \middle| \, \mathscr{H}_f \right\rangle. \tag{4.10}$$

Note that for an averaging volume Ω with dimension $\Delta y \leqslant \Delta x$, the fluid velocity constructed from (4.10) can be compared to the corresponding fluid velocity obtained in the DNS in order to assess errors arising from the interpolation of the fluid velocity from neighbouring grid points to the particle positions, in addition to effects arising from any bias in the particle concentration with the volume Ω.

Given an ensemble of realizations $\mathscr{N}_p$, each with N_p particles, the above relations for the MEPVF are approximated as

$$\widetilde{n}_p^*(\boldsymbol{x}, t, \mathscr{H}_f) = \frac{1}{\mathscr{N}_p} \sum_{\mathscr{N}_p} \sum_{m=1}^{N_p} \chi_p^{(m)*}(\boldsymbol{x}, t, \mathscr{H}_p | \mathscr{H}_f), \tag{4.11}$$

where $\widetilde{n}_p^*(\boldsymbol{x}, t)(\Delta y)^3$ represents the instantaneous number of particles within the volume $\Omega(\boldsymbol{x})$. The velocity is obtained via

$$\widetilde{v}_p^*(\boldsymbol{x}, t, \mathscr{H}_f) = \frac{1}{\widetilde{n}_p^*(\boldsymbol{x}, t, \mathscr{H}_f)} \frac{1}{\mathscr{N}_p} \sum_{\mathscr{N}_p} \sum_{m=1}^{N_p} \boldsymbol{v}_p^{(m)}(t) \chi_p^{(m)*}(\boldsymbol{x}, t, \mathscr{H}_p | \mathscr{H}_f), \tag{4.12}$$

where $\chi_p^{(m)*}(\boldsymbol{x}, t, \mathscr{H}_{f\&p}) = 1/\Omega(\boldsymbol{x})$ if the centre of particle m is within the volume $\Omega(\boldsymbol{x})$ at time t, and $\chi_p^{(m)*}(\boldsymbol{x}, t, \mathscr{H}_p | \mathscr{H}_f) = 0$ otherwise. The fluid velocity along particle trajectories is approximated by

$$\boldsymbol{u}^*(x, t) = \frac{1}{\widetilde{n}_p^*(\boldsymbol{x}, t, \mathscr{H}_f)} \frac{1}{\mathscr{N}_p} \sum_{\mathscr{N}_p} \sum_{m=1}^{N_p} \boldsymbol{u}\big(\boldsymbol{x}_p^{(m)}(t), t\big) \chi_p^{(m)*}(\boldsymbol{x}, t, \mathscr{H}_p | \mathscr{H}_f). \tag{4.13}$$

The accuracy of the instantaneous Eulerian quantities computed using the above formulae, i.e. the variables with the $*$ superscripts, is dependent upon the sample size $\mathscr{N}_s$ employed in the averaging process. With averaging over both space and $\mathscr{N}_p$ realizations, the sample size is written as

$$\mathscr{N}_s(\boldsymbol{x}, t) = \mathscr{N}_p \widetilde{n}_p^*(\boldsymbol{x}, t, \mathscr{H}_f) \Omega(\boldsymbol{x}), \tag{4.14}$$

showing that the number of samples $\mathscr{N}_s$ in volume $\Omega(\boldsymbol{x})$ is given by the particle population within the volume $\Omega(\boldsymbol{x})$ at time t over all $\mathscr{N}_p$ realizations. Note that if $\mathscr{N}_s$ is very large, (4.11), (4.12), and (4.13) will be accurate approximations of the instantaneous mesoscopic Eulerian properties of the particulate phase. If the sample $\mathscr{N}_s(\boldsymbol{x}, t)$ is not large ($\mathscr{N}_s(\boldsymbol{x}, t) = \{0; 1\}$), then statistics of the particulate phase will be representative of the complete particle velocity, rather than the MEPVF. Note that $\mathscr{N}_s(\boldsymbol{x}, t) = \{0; 1\}$ implies that two-point statistics are relevant only for $r \geqslant \Delta y$. Variation in the sample size then enables verification of theoretical relations such as (3.25).

One- and two-point statistics are computed according to the relations in § 3.2. For example, the turbulent kinetic energy of the MEPVF is approximated as

$$\widetilde{q}_p^{2*} = \frac{1}{2} \frac{\langle \widetilde{n}_p^*(\boldsymbol{x}, t, \mathscr{H}_f) \widetilde{v}_{p,i}'^*(\boldsymbol{x}, t, \mathscr{H}_f) \widetilde{v}_{p,i}'^*(\boldsymbol{x}, t, \mathscr{H}_f) \rangle}{\langle \widetilde{n}_p^*(\boldsymbol{x}, t, \mathscr{H}_f) \rangle} \tag{4.15}$$

where $\widetilde{v}_{p,i}'^* = \widetilde{v}_{p,i}^* - V_{p,i}$. The radial distribution function g^{pp} is calculated from

$$g^{pp*}(\boldsymbol{r}) = \frac{\langle \widetilde{n}_p^*(\boldsymbol{x}, t, \mathscr{H}_f) \widetilde{n}_p^*(\boldsymbol{x} + \boldsymbol{r}, t, \mathscr{H}_f) \rangle}{\langle \widetilde{n}_p^*(\boldsymbol{x}, t, \mathscr{H}_f) \rangle \langle \widetilde{n}_p^*(\boldsymbol{x} + \boldsymbol{r}, t, \mathscr{H}_f) \rangle}. \tag{4.16}$$

Two-point velocity correlations, for example the particle–particle correlations, are calculated via

$$R_{ij}^{pp*}(\boldsymbol{r}) = \frac{\langle \widetilde{n}_p^*(\boldsymbol{x}) \widetilde{v}_{p,i}'^*(\boldsymbol{x}) \widetilde{n}_p^*(\boldsymbol{x} + \boldsymbol{r}) \widetilde{v}_{p,j}'^*(\boldsymbol{x} + \boldsymbol{r}) \rangle}{\langle \widetilde{n}_p^*(\boldsymbol{x}) \widetilde{n}_p^*(\boldsymbol{x} + \boldsymbol{r}) \rangle}. \tag{4.17}$$

Note that the dependence of the mesoscopic Eulerian quantities on $\mathscr{H}_f$ and t is omitted from the above.

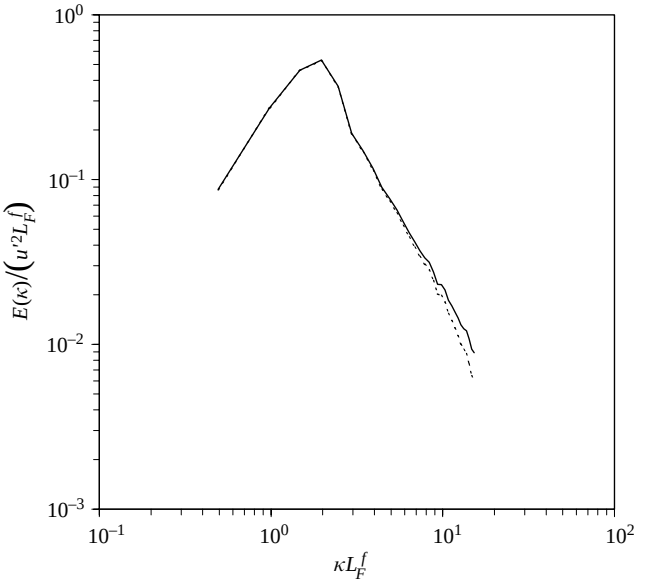

FIGURE 4. Comparison of the fluid turbulence energy spectrum computed on the grid to that obtained following massless particle trajectories and obtained using (4.13). ——, fluid energy spectrum on the grid; – – – –, fluid energy spectrum obtained from the velocity obtained using (4.13). LES prediction at $Re_L = 700$.

5. Validation of the numerical approach for assessing the MEF

Prior to applying the method described in §4.4 to finite-inertia particles, the approach is assessed for fluid-element motion. Shown in figure 4 is a comparison of the energy spectrum obtained from the fluid flow solution on the grid to that obtained from the velocity field computed using (4.13), i.e. following fluid element trajectories. The agreement in the spectra at low wavenumbers is very good, with more visible differences apparent at the high wavenumbers. The larger differences at the higher wavenumbers arises from the filtering effect of the interpolation used to determine the fluid velocity along particle trajectories (e.g. see Boivin *et al.* 1998). This discrepancy is highlighted in the LES at large turbulence Reynolds number since $\kappa_{max}\eta$ is substantially below unity (cf. table 1). For larger values of the parameter $\kappa_{max}\eta > 1$, as in the DNS, the differences in the spectra shown in figure 4 are smaller.

Variations in the accuracy and scale of resolution can be considered via changes in Δy and $\mathcal{N}_s$. For a fixed particle sample size N_p, variation in Δy implies corresponding variations in $\mathcal{N}_s$. In the following, different values of the combination $(\Delta y; \mathcal{N}_s)$ are considered, with changes in $\mathcal{N}_s$ achieved via variations in N_p as well as Δy.

Shown in figure 5 is the influence of the volume size over which the particulate-phase number density and velocity are resolved as well as the effect of the sample size $\mathcal{N}_s$ on the radial distribution function. Variation in $\langle \mathcal{N}_s \rangle$ enables *a posteriori* verification of the theoretical relation (3.22) developed in Part I. Profiles are shown for a range of particle Stokes numbers, $St = \tau_{fp}^F / T_L$; the results shown in the figure are from the DNS at $Re_L = 140$, and the radial distribution function $g^{pp*}(r)$ is computed using (4.16). The profiles shown in the figure were obtained using volumes Ω with resolution identical to that used for the DNS, i.e. $\Delta y = \Delta x$ and finer by more than a factor of two, $\Delta y = 3\Delta x/8$. For the larger volume, the average sample of particles per

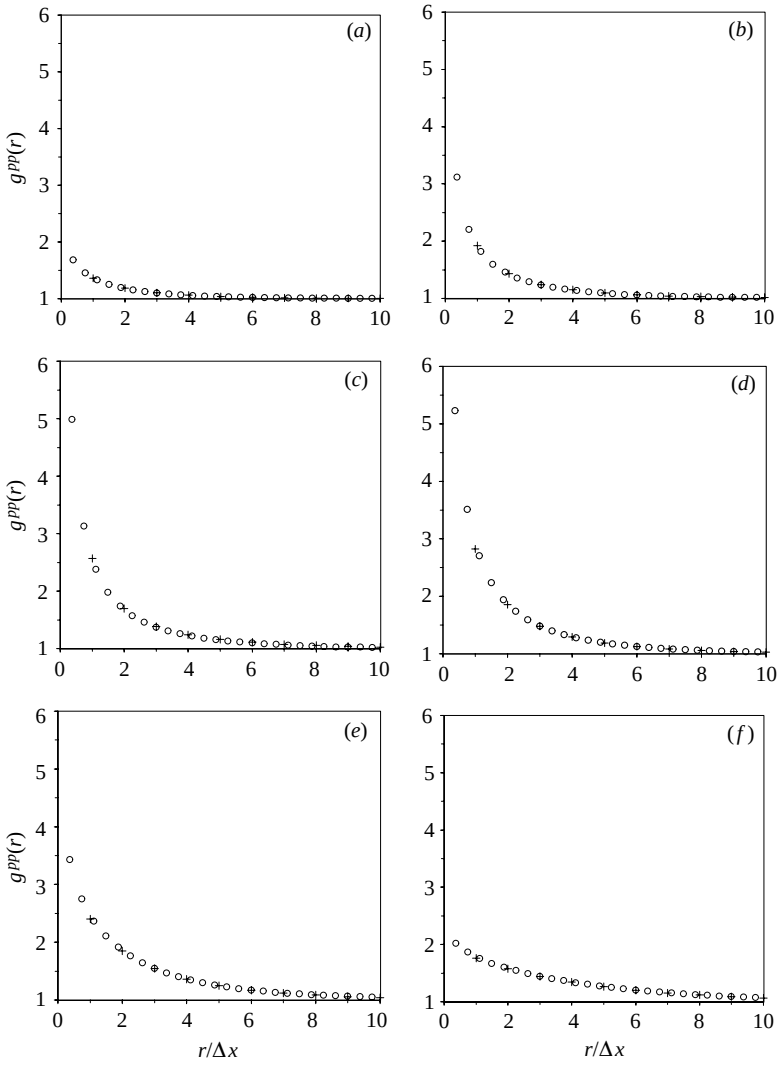

FIGURE 5. Influence of volume size and sample size on the radial distribution function $g^{pp}(r)$. Profiles shown for Stokes number, $St = \tau_{fp}^F / T_L$, considered in the 96^3 DNS, $Re_L = 140$. (*a*) $St = 0.022$; (*b*) $St = 0.05$; (*c*) $St = 0.087$; (*d*) $St = 0.134$; (*e*) $St = 0.256$; (*f*) $St = 0.5$. ○, $g^{pp}(r)$ obtained using volumes Ω with dimension $\Delta y = 3\Delta x/8$ and $\langle \mathcal{N}_s \rangle = 0.6$; +, $g^{pp}(r)$ obtained using volumes Ω with dimension $\Delta y = \Delta x$ and $\langle \mathcal{N}_s \rangle = 11.3$.

cell is $\langle \mathcal{N}_s \rangle = 11.3$, while for the smaller volume the average sample is $\langle \mathcal{N}_s \rangle = 0.6$. An important feature is that figure 5 shows that g^{pp*} is not sensitive to the parameter $\mathcal{N}_s$, in turn consistent with the theoretical relation (3.22). Further, comparison between g^{pp*} obtained on the larger grid $\Delta y = \Delta x$ to that obtained on the finer mesh with $\Delta y = 3\Delta x/8$ shows that $g^{pp*}(r)$ is represented with comparable accuracy for $r \geqslant \Delta y$.

Figure 5 shows that the change with St in the radial distribution function is not monotonic, with peak values away from unity for the intermediate Stokes numbers around 0.10. Scaling of the Stokes number using Kolmogorov variables shows the peak occurring for Stokes numbers close to unity, in agreement with Sundaram & Collins (1997) and Reade & Collins (2000), among others. As discussed in Wang & Maxey

(1993), low-inertia particles tend to passively follow the turbulent motion of the fluid and preferential concentration into low-vorticity or high-strain-rate regions is weak. For very large Stokes numbers, particle motion is relatively unaffected by interactions with the turbulent carrier flow and effects of preferential concentration are again not substantial. Between these limiting cases, effects of preferential concentration become apparent, as shown in the figure with the radial distribution function larger than unity at small distances r. The variations of the radial distribution function with distance r are closely associated with the shape of particle clusters in the flow. If, for example, a large number of particles are clustered into thin structures, then there will be strong variations in $g^{pp}(r)$ for small r (e.g. see Reade & Collins 2000). For substantially non-uniform distributions of the particles, the spatial variations of the instantaneous particle number density $\widetilde{n}_p$ are in turn also quite large. Consequently, the accuracy to which properties of the MEPVF can be recovered from the volume averages decreases with increasing effects of particle segregation by turbulent structures.

Shown in figure 6 is the effect of the parameters Δy and $\mathscr{N}_s$ on the longitudinal two-point correlations: the fluid–particle velocity correlations $F^{fp*}(r)$ and the particle–particle velocity correlations $F^{pp*}(r)$. Similar to the behaviour observed in the radial distribution function, the figure shows that the correlations $F^{pp*}(r)$ and $F^{fp*}(r)$ are not sensitive to the sample size $\mathscr{N}_s$, a result that is in agreement with the relations (3.23) and (3.24) developed in Part I. Figure 6 also shows that the velocity correlations are accurate for $\Delta y \leqslant \Delta x$, consistent with the assumption of negligible variations in the spatial features of the particulate-phase properties at scales smaller than the smallest scales of the fluid flow. It should be noted, however, that a small dependence on Δy is apparent for $r < 2\Delta y$ for particles that exhibit strong effects of preferential concentration, e.g. as shown in figure 5 for $St = 0.134$ and also observed in the fluid–fluid velocity correlations $F^{ff*}(r)$ in figure 6.

Two-point velocity correlations are displayed in figure 7 for finite-inertia particles that do not exhibit strong effects of preferential concentration ($St = 3.15$), the particular curves being obtained from the LES at $Re_L = 700$. The correlations are obtained for different values of the average particle sample $\langle \mathscr{N}_s \rangle$ ranging from 0.017 to 38.1, the largest sample size being adequate for obtaining an accurate description of the MEPVF and QBVD. The results in the figure again confirm that $F^{pp*}(r)$, $F^{fp*}(r)$ and $F^{ff*}(r)$ do not depend on the parameter $\mathscr{N}_s$. For Δy smaller than the mesh size Δx used for solution of the Navier–Stokes equations, the velocity correlations are accurate with no dependence on Δy. For $\Delta y > \Delta x$, the small scales of the fluid turbulence are not captured by $F^{ff*}(r)$, and as shown by figure 7, $F^{ff*}(r)$ differs from the actual correlation $F^{ff}(r)$ for small separations r. In contrast, this discrepancy is not yet apparent in the correlations $F^{pp*}(r)$ and $F^{fp*}(r)$ because the spacing Δy remains smaller than the smallest scales of the MEPVF.

Considering the independence of the two-point velocity correlations of the parameter $\mathscr{N}_s$, the numerical results confirm that the MEPVF accounts completely for the spatial correlations of the particulate phase, i.e. in agreement with the theoretical relations (3.23), (3.24), and (3.25), for $r \geqslant d_p$,

$$F^{pp}(r) = \widetilde{F}^{pp}(r), \qquad F^{fp}(r) = \widetilde{F}^{fp}(r), \qquad F^{ff}(r) = \widetilde{F}^{ff}(r). \tag{5.1}$$

The numerical results show that, in the limit $r/L_F^f \to 0$, the two-point velocity correlations $\widetilde{F}^{fp}(r)$ and $\widetilde{F}^{ff}(r)$ tend to the one-point velocity correlations $\widetilde{q}_{fp}/3$ and $2\widetilde{q}^2_{f@p}/3$, respectively. Furthermore, the theoretical relations $\widetilde{q}_{fp} = q_{fp}$ and $\widetilde{q}^2_{f@p} = q^2_{f@p}$ have also been confirmed from the numerical simulations. This in turn leads to the following

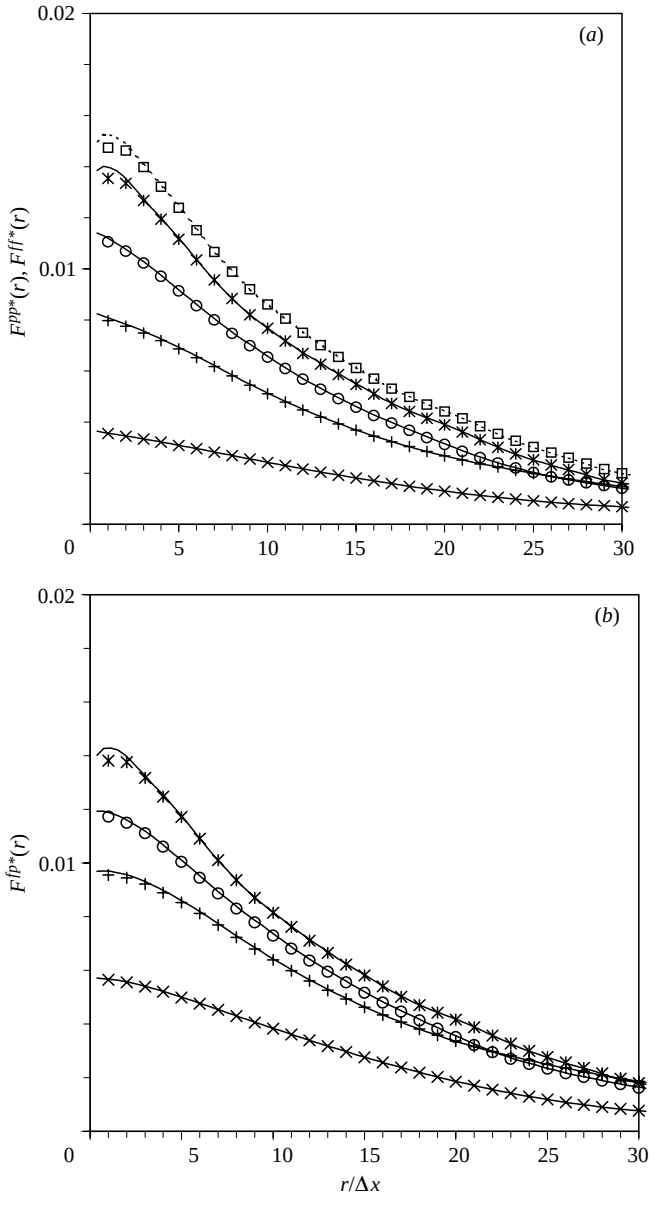

FIGURE 6. Influence of volume size and sample size on (*a*) the Eulerian particle–particle $F^{pp*}(r)$ and (*b*) fluid–particle $F^{fp*}(r)$ velocity correlations. Profiles obtained from 96^3 DNS at $Re_L = 140$. ——, $\Delta y = 3\Delta x/8$, $\langle \mathcal{N}_s \rangle = 0.12$; symbols are for $\Delta y = \Delta x$, $\langle \mathcal{N}_s \rangle = 11.3$: *, $\tau^F_{fp}/T_L = 0.134$; ○, $\tau^F_{fp}/T_L = 0.256$; +, $\tau^F_{fp}/T_L = 0.5$; ×, $\tau^F_{fp}/T_L = 1.5$. The fluid–fluid velocity correlations sampled along particle trajectories for $\tau^F_{fp}/T_L = 0.134$ are also shown using – – – – for $\Delta y = 3\Delta x/8$ and □ for $\Delta y = \Delta x$ in (*a*).

relations:

$$\lim_{r/L^f_F \to 0} \widetilde{F}^{fp}(r) = \widetilde{q}_{fp}/3 = q_{fp}/3, \tag{5.2}$$

$$\lim_{r/L^f_F \to 0} \widetilde{F}^{ff}(r) = 2\widetilde{q}^2_{f@p}/3 = 2q^2_{f@p}/3. \tag{5.3}$$

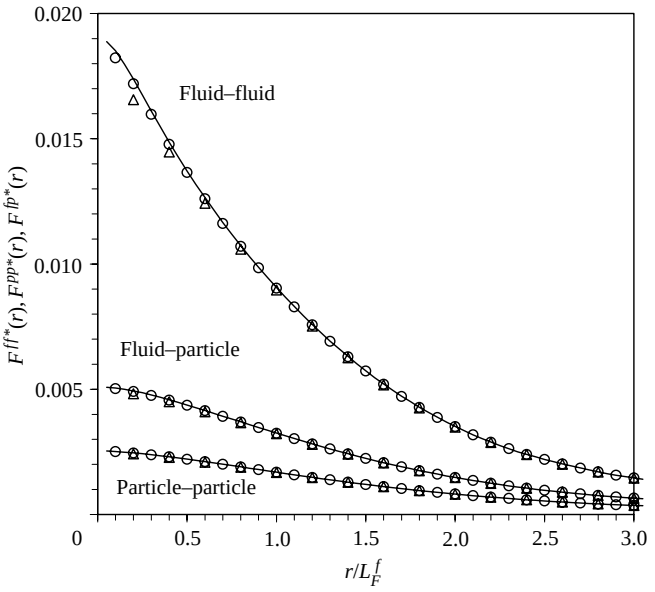

FIGURE 7. Influence of volume size and sample size on the fluid–fluid, fluid–particle, and particle–particle Eulerian velocity correlations. Profiles obtained from LES at $Re_L = 700$, $St = 3.15$. ——, $\Delta y = 3\Delta x/8$, $\langle \mathcal{N}_s \rangle = 0.017$; ○, $\Delta y = 3\Delta x/4$, $\langle \mathcal{N}_s \rangle = 4.7$. △, $\Delta y = 3\Delta x/2$, $\langle \mathcal{N}_s \rangle = 38.1$.

An additional important result demonstrated by the simulations is that the particle–particle two-point velocity correlations remain smaller than the fluid–particle correlation (cf. figure 7) and in the limit of the separation r going to zero,

$$\lim_{r/L_F^f \to 0} \widetilde{F}^{pp}(r) = 2\widetilde{q}_p^2/3 \leqslant 2q_p^2/3. \tag{5.4}$$

6. Measured characteristics of the MEPVF and QBVD

6.1. *Kinetic energy of the MEPVF and QBVD*

The QBVD represents a random contribution to the motion of a finite-inertia particle, an effect that can be demonstrated through consideration of the effect of the initial particle velocity on the subsequent development of the kinetic energy of the MEPVF and QBVD. This effect is shown in figure 8. Three different initial conditions for the particle velocity are shown in the figure: (i) the initial particle velocity equal to the fluid velocity at the particle position, (ii) zero initial particle velocity, and (iii) a random initial particle velocity sampled from a Gaussian distribution with zero mean and variance close to $2q^2/3$. For each initial condition, the particles are evolved in the same realization of the fluid flow; the results shown in the figure are from the 96^3 DNS at $Re_L = 140$. Note also that the fluid flow simulation was first integrated to a statistical equilibrium prior to integration of the particulate phase. The influence of the initial conditions on the temporal evolution of the kinetic energy of the MEPVF and QBVD is shown for $St = 0.81$.

For the first case (i), the initial particle velocities possess the same spatial correlation as the fluid elements from which the initial velocity was specified. The quasi-Brownian contribution to the particle velocity for this case is zero, i.e. $\delta q_p^2 = 0$. The figure shows

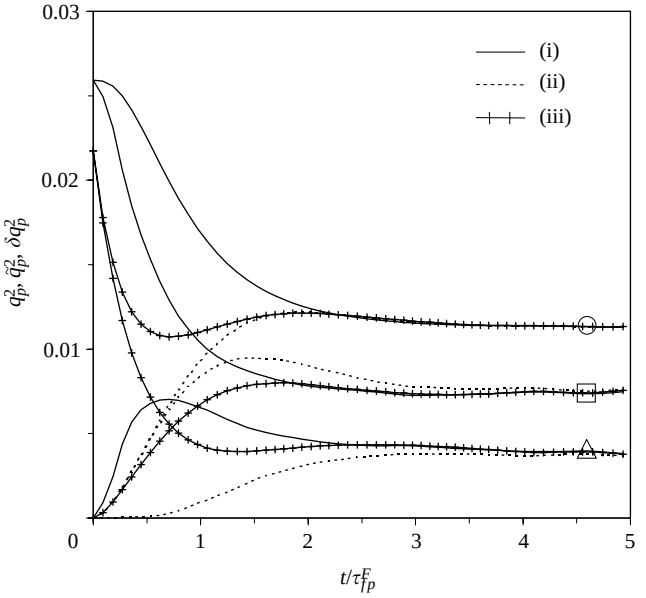

FIGURE 8. Influence of the initial velocity on the kinetic energy of the MEPVF and QBVD. ○, q_p^2; □, $\widetilde{q}_p^2$; △, δq_p^2. Particle positions are initially random throughout the computational domain. Initial velocities: (i) particle velocity equal to the fluid velocity at the particle position, (ii) zero velocity, (iii) random velocities sampled from a Gaussian distribution with zero mean and variance equal to u'^2. Results from the 96^3 DNS at $Re_L = 140$, $St = 0.81$.

that the total kinetic energy q_p^2 decreases to its equilibrium value within about $3\tau_{fp}^F$. The kinetic energy of the MEPVF decreases more rapidly than does q_p^2 while the energy of the QBVD increases. Equilibrium values for $\widetilde{q}_p^2$ and δq_p^2 are also attained after about $3\tau_{fp}^F$. For case (ii) the initial particle velocities correspond to kinetic energies $\widetilde{q}_p^2 = q_p^2 = 0$ and $\delta q_p^2 = 0$; for case (iii) the initial particle velocities have no spatial correlation, i.e. $\delta q_p^2 = q_p^2$. For each case, the energy of the MEPVF and QBVD reaches the same equilibrium state, the transient being again about $3\tau_{fp}^F$. Figure 8 shows that the QBVD is a physical contribution to the particle velocity distribution resulting from the inertial bias in particle trajectories.

The equilibrium values of the kinetic energy of the MEPVF and QBVD normalized by the total particle kinetic energy are shown in figure 9. For small response times, particles tend to move as fluid elements and consistent with the scalar limiting case the simulations show that the kinetic energy of the QBVD tends to zero. With increasing inertia, particles do not adapt as rapidly to the local fluid motions, and the simulations show the fraction of kinetic energy residing in the QBVD, $\delta q_p^2/q_p^2$, increases while the fraction residing in the MEPVF decreases. For response times $\tau_{fp}^F \approx T_L$, the contribution of the QBVD to the particle kinetic energy is approximately 30% of the total. In the limit of very large inertia, particle motion will be mainly driven by the QBVD, with negligible energy in the MEPVF. Consistent with the work of Abrahamson (1975), in the large-inertia limit particle transport will be stochastically equivalent to a Brownian motion. In addition, the particle velocity distribution as well as the distribution of the relative velocity between two particles will be Gaussian in the large-inertia limit (e.g. see Laviéville, Deutsch & Simonin 1995).

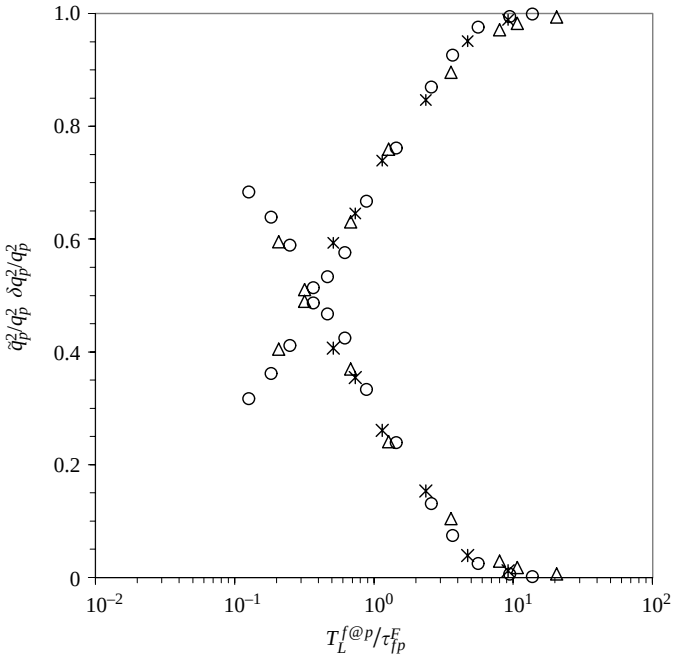

FIGURE 9. Effect of particle inertia on the kinetic energy of the MEPVF and QBVD. Values of the ordinate tending to 1 (0) for large values of the abscissa identify $\widetilde{q}_p^2/q_p^2$ ($\delta q_p^2/q_p^2$). ○, 128^3 DNS at $Re_L = 110$; *, 96^3 DNS at $Re_L = 140$; △, LES at $Re_L = 700$.

An important result apparent in figure 9 is that the evolution of the kinetic energy of the MEPVF and QBVD are similar for both DNS, i.e. at 128^3 and $Re_L = 110$, 96^3 and $Re_L = 140$. These calculations employ different parameters for the forcing scheme used to maintain a statistically stationary flow. This in turn further illustrates that the QBVD is not an artifact of the stochastic process evolving from the forcing, but is a physical feature arising because of the inertia of the particles. Furthermore, for large-inertia particles that are quite unresponsive to the small-scale fluid turbulent motions, the evolution of the kinetic energy of the MEPVF and QBVD is accurately predicted in the LES, as illustrated via the large-scale normalization (cf. figure 9). This further reinforces the result that quantities such as the total particle kinetic energy are dominated by the large-scale motions of the fluid. In the present context, the long-time statistics of the MEPVF and QBVD are controlled by the interaction of particles with the large turbulent scales of the fluid.

The mean values, for the particle fluctuating motion, of the total kinetic energy (q_p^2), MEPVF ($\widetilde{q}_p^2$), and QBVD (δq_p^2) normalized by the fluid kinetic energy following particle trajectories $q_{f@p}^2$ are shown in figure 10. For the flow fields under consideration in this study – statistically stationary homogeneous and isotropic particle-laden turbulence with particle motion given by (4.2) – simulation results may be evaluated using the theoretical predictions from Tchen (1947) assuming an exponential shape for the fluid autocorrelation function measured along the particle path (Deutsch & Simonin 1991):

$$q_p^2 = \tfrac{1}{2} q_{fp}, \qquad q_{fp} = 2\frac{\eta_r}{1+\eta_r} q_{f@p}^2 \tag{6.1}$$

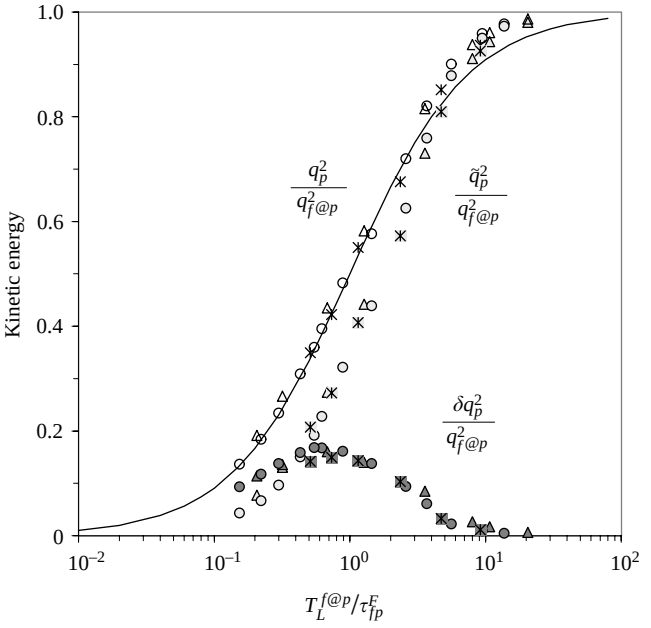

FIGURE 10. Effect of particle inertia on the particulate-phase kinetic energy. ○, 128^3 DNS at $Re_L = 110$; *, 96^3 DNS at $Re_L = 140$; △, LES at $Re_L = 700$. ——, prediction of the total particulate-phase kinetic energy using the theoretical relation (6.1).

with the time-scale ratio $\eta_r = T_L^{f@p}/\tau_{fp}^F$. As shown by figure 10, the dependence of q_p^2 on particle inertia is accurately predicted using (6.1) for large- and intermediate-inertia particles; deviations from the simulation results are observed for smaller response times due to effects of inertial bias in particle motion. The calculations show a maximum in δq_p^2 for $\tau_{fp}^F \approx T_L$. This maximum represents a balance between the reduction of the total turbulent kinetic energy q_p^2 and the increase of the QBVD contribution that arises with increasing inertia. Note that figure 10 also shows that the kinetic energy of the MEPVF decays more rapidly with increases in particle inertia than observed for q_p^2. This feature not only provides additional evidence for the existence of the QBVD, but is also indicative of a transfer of energy from the MEPVF towards the QBVD, as shown in the next section using the transport equations governing $\widetilde{q}_p^2$ and δq_p^2.

The ratio of the kinetic energy of the mesoscopic field to the total particulate-phase kinetic energy is shown in figure 11, plotted against the ratio of the total particle-phase kinetic energy to the fluid kinetic energy following particle trajectories. Also shown using the solid line in the figure is the relationship corresponding to a square-root growth of $\widetilde{q}_p^2/q_p^2$ with $q_p^2/q_{f@p}^2$. Figure 11 shows that the simulation results follow the square-root dependence reasonably closely for both sets of DNS results and LES predictions.

6.2. *Eulerian transport equations for the mesoscopic field*

As discussed in the previous section, figure 10 provides evidence for both the existence of the QBVD and the transfer of particulate-phase kinetic energy from the correlated motions towards the quasi-Brownian component. Additional insight into the partitioning of the particle velocity can be gained by consideration of the

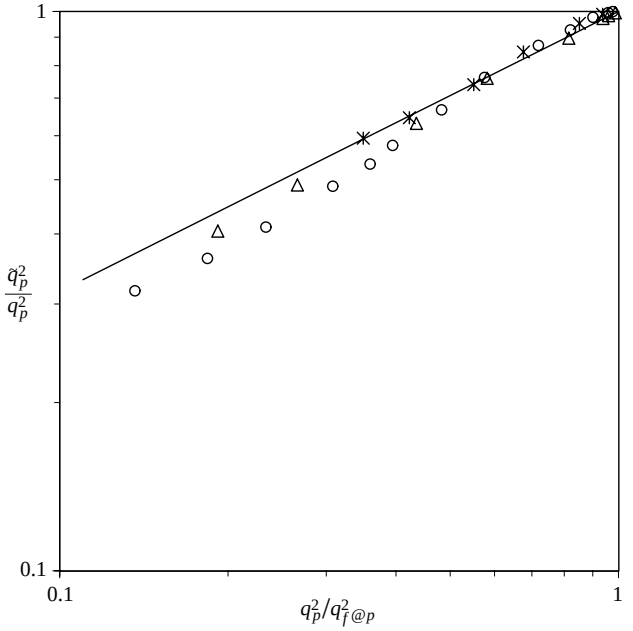

FIGURE 11. Ratio of the mean kinetic energy of the MEPVF, $\widetilde{q}_p^2$, to the total particulate-phase kinetic energy, q_p^2. The ratio of q_p^2 to the fluid kinetic energy following particle trajectories is plotted along the horizontal axis; the solid line corresponds to a square-root growth of $\widetilde{q}_p^2$. ○, 128^3 DNS at $Re_L = 110$; *, 96^3 DNS at $Re_L = 140$; △, LES at $Re_L = 700$.

transport equations for the particle velocity field. The relevant equations are derived in this section.

Eulerian transport equations governing the evolution of the particulate phase can be derived from the kinetic equation satisfied by the p.d.f. $\widetilde{f}_p^{(1)}$,

$$\frac{\partial \widetilde{f}_p^{(1)}}{\partial t} + \frac{\partial}{\partial x_j}\left[c_{p,j}\widetilde{f}_p^{(1)}\right] + \frac{\partial}{\partial c_{p,j}}\left[\frac{F_j}{m_p}\widetilde{f}_p^{(1)}\right] = 0, \tag{6.2}$$

where F_j represents the external force acting on the particle and m_p is the particle mass. Moments of (6.2) yield transport equations for local and instantaneous quantities, and the relations developed below correspond to a fluid force acting on the particle that is written in the form $F_j = -m_p(c_{p,j} - u_j)/\tau_p$ where τ_p is a function of the particle Reynolds number, e.g. as illustrated by (4.2) and (4.3). In the Stokes regime, the force F_j varies linearly with respect to the particle-to-fluid relative velocity, the relaxation time is given by $\tau_p = \rho_p d_p^2/(18\rho\nu)$ (ν is the fluid kinematic viscosity), and the averaged fluid force in the Eulerian transport equations can be written explicitly in terms of the mesoscopic particle properties. If the force F_j is not linear it is possible to generalize the proposed approach, consistent with the introduction of the mean particle relaxation time τ_{fp}^F given in (4.4), by introducing an averaged particle relaxation time $\widetilde{\tau}_p = \rho_p d_p^2/(18\nu)/\langle f_D|\boldsymbol{x} = \boldsymbol{x}_p(t); \mathscr{H}_f\rangle$ and by neglecting the correlations between the fluctuations of the drag coefficient and of the particle relative velocity. The mean particle relaxation time (4.4) is related to $\widetilde{\tau}_p$ via $1/\tau_{fp}^F = \langle 1/\widetilde{\tau}_p\rangle_p$.

Using (3.2), (3.3), and (6.2), the number density $\widetilde{n}_p$ evolves according to

$$\frac{\partial \widetilde{n}_p}{\partial t} + \frac{\partial}{\partial x_i}[\widetilde{n}_p \widetilde{v}_{p,i}] = 0. \tag{6.3}$$

Similarly, the mesoscopic Eulerian velocity $\widetilde{v}_{p,i}$ satisfies

$$\widetilde{n}_p \frac{\partial \widetilde{v}_{p,i}}{\partial t} + \widetilde{n}_p \widetilde{v}_{p,j} \frac{\partial \widetilde{v}_{p,i}}{\partial x_j} = \widetilde{n}_p g_i - \widetilde{n}_p \left[\frac{\widetilde{v}_{p,i} - u_i}{\widetilde{\tau}_p} \right] - \frac{\partial}{\partial x_j}[\widetilde{n}_p \delta\widetilde{\sigma}_{p,ij}], \tag{6.4}$$

where g_i is the acceleration due to gravity. The last term in (6.4) accounts for the action of the QBVD on the MEPVF where $\delta\widetilde{\sigma}_{p,ij}$ is the 'kinetic stress tensor' of the QBVD. The trace of this tensor can be used to define a quasi-Brownian pressure, an effect that will induce dispersion of the number density $\widetilde{n}_p$, and the non-diagonal part of $\delta\widetilde{\sigma}_{p,ij}$ will induce a dissipation of the MEPVF. The transport of the kinetic energy of the QBVD $\delta\widetilde{\theta}_p = \delta\widetilde{\sigma}_{p,ii}/2$ can also be derived from (6.2), leading to

$$\widetilde{n}_p \frac{\partial \delta\widetilde{\theta}_p}{\partial t} + \widetilde{n}_p \widetilde{v}_{p,i} \frac{\partial \delta\widetilde{\theta}_p}{\partial x_i} = -\widetilde{n}_p \delta\widetilde{\sigma}_{p,ij} \frac{\partial \widetilde{v}_{p,i}}{\partial x_j} - 2\frac{\widetilde{n}_p}{\widetilde{\tau}_p} \delta\widetilde{\theta}_p - \frac{\partial}{\partial x_i}[\widetilde{n}_p \delta\widetilde{Q}_{p,i}]. \tag{6.5}$$

The first term on the right-hand side of (6.5) accounts for the transfer of energy from the MEPVF towards the quasi-Brownian component. As shown by (6.5), the production of kinetic energy occurs via interaction with the velocity gradients of the MEPVF. It is important to note that the kinetic energy of the quasi-Brownian motions is not produced via direct interactions with the carrier fluid flow. The second term accounts for the effect of the fluid interaction with the particles and is a purely dissipative contribution to the QBVD. The last term represents transport due to the triple-velocity correlations where $\delta\widetilde{Q}_{p,i} = \langle \delta v_{p,i} \delta v_{p,j} \delta v_{p,j} | \boldsymbol{x} = \boldsymbol{x}_p(t); \mathscr{H}_f \rangle / 2$ is the contracted third-order correlation of the QBVD.

6.3. *Mean kinetic energy transport equations for the MEPVF and QBVD*

The interactions between the mean kinetic energy of the MEPVF and QBVD are derived using the Eulerian transport equations above that describe the local and instantaneous MEPVF. The mean kinetic energy of the fluctuating component of the MEPVF, $\widetilde{q}_p^2$, is repeated from (3.9) for convenience,

$$n_p \widetilde{q}_p^2 = \tfrac{1}{2} \langle \widetilde{n}_p \widetilde{v}'_{p,i} \widetilde{v}'_{p,i} \rangle = \tfrac{1}{2} n_p \langle \widetilde{v}'_{p,i} \widetilde{v}'_{p,i} \rangle_p, \tag{6.6}$$

where n_p is the mean number density. The balance equation for $\widetilde{q}_p^2$ can be derived by averaging over all two-phase flow realizations the vector product of $\widetilde{v}'_{p,i}$ with (6.4),

$$\begin{aligned} n_p \frac{\partial \widetilde{q}_p^2}{\partial t} + n_p V_{p,i} \frac{\partial \widetilde{q}_p^2}{\partial x_i} = &-\frac{\partial}{\partial x_j} \frac{1}{2} [n_p \langle \widetilde{v}'_{p,i} \delta\widetilde{\sigma}_{p,ij} \rangle_p + n_p \langle \widetilde{v}'_{p,i} \widetilde{v}'_{p,i} \widetilde{v}'_{p,j} \rangle_p] \\ &- \frac{n_p}{\tau_{fp}^F} [2\widetilde{q}_p^2 - q_{fp}] - n_p \langle \widetilde{v}'_{p,i} \widetilde{v}'_{p,j} \rangle_p \frac{\partial V_{p,i}}{\partial x_j} - n_p \widetilde{\epsilon}_p. \end{aligned} \tag{6.7}$$

The dissipation rate of the mesoscopic field has been introduced into the last term of (6.7) and takes the form

$$\widetilde{\epsilon}_p = -\left\langle \delta\widetilde{\sigma}_{p,ij} \frac{\partial \widetilde{v}'_{p,i}}{\partial x_j} \right\rangle_p. \tag{6.8}$$

For the QBVD, the mean kinetic energy of the residual component of the particulate velocity is rewritten from (3.11),

$$n_p \delta q_p^2 = \tfrac{1}{2} \langle \widetilde{n}_p \delta v_{p,i} \delta v_{p,i} \rangle = n_p \langle \delta\widetilde{\theta}_p \rangle_p. \tag{6.9}$$

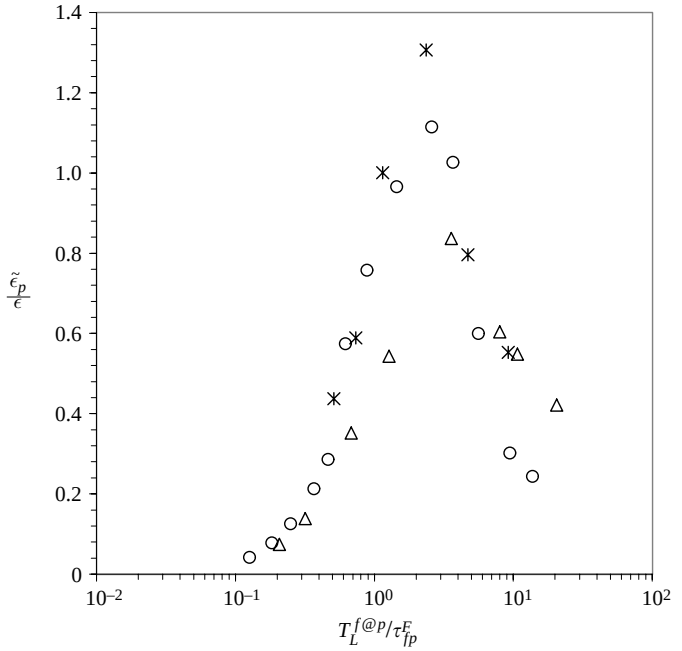

FIGURE 12. Effect of particle inertia on the dissipation rate of the MEPVF, $\widetilde{\epsilon}_p$. ○, 128^3 DNS at $Re_L = 110$; ∗, 96^3 DNS at $Re_L = 140$; △, LES at $Re_L = 700$.

Averaging (6.5) yields the transport of the mean kinetic energy of the quasi-Brownian motion,

$$n_p \frac{\partial \delta q_p^2}{\partial t} + n_p V_{p,i} \frac{\partial \delta q_p^2}{\partial x_i} = -\frac{\partial}{\partial x_j}[n_p \langle \delta \widetilde{Q}_{p,i} \rangle_p + n_p \langle \widetilde{v}'_{p,j} \delta \widetilde{\theta}_p \rangle_p] - \frac{n_p}{\tau_{fp}^F} 2\delta q_p^2 - n_p \langle \delta \widetilde{\sigma}_{p,ij} \rangle_p \frac{\partial V_{p,i}}{\partial x_j} + n_p \widetilde{\epsilon}_p. \quad (6.10)$$

Important to note in the above is that the dissipation of the kinetic energy of the MEPVF in (6.7) corresponds to production of the quasi-Brownian kinetic energy in (6.10).

The relations governing kinetic energy transport can be simplified for the current simulations of statistically stationary, homogeneous and isotropic turbulence. The transport of the mean mesoscopic turbulent kinetic energy (6.7) reduces to

$$-\frac{1}{\tau_{fp}^F}[2\widetilde{q}_p^2 - q_{fp}] - \widetilde{\epsilon}_p = 0, \quad (6.11)$$

and the mean kinetic energy of the quasi-Brownian motion (6.10) becomes

$$-\frac{1}{\tau_{fp}^F} 2\delta q_p^2 + \widetilde{\epsilon}_p = 0. \quad (6.12)$$

Values of $\widetilde{\epsilon}_p$ normalized by the dissipation rate of the fluid turbulence ϵ are shown in figure 12. For small relaxation times the figure shows that the ratio of $\widetilde{\epsilon}_p$ to the fluid dissipation rate is small, corresponding to the regime in which most of the kinetic energy of the particles resides in the correlated motion and for which there is relatively little transfer to the quasi-Brownian component (cf. figure 10). For large

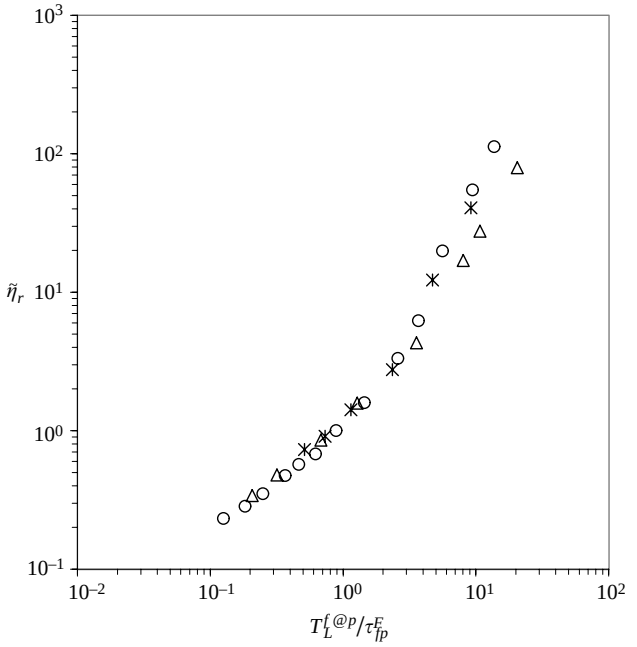

FIGURE 13. Effect of particle inertia on the time-scale ratio, $\widetilde{\eta}_r$. ○, 128^3 DNS at $Re_L = 110$; *, 96^3 DNS at $Re_L = 140$; △, LES at $Re_L = 700$.

particle response times, figure 12 shows that the transfer of particulate-phase kinetic energy from the MEPVF to the QBVD is smaller than at intermediate response times, a consequence of the relatively low kinetic energy of the particles for large relaxation times. In the intermediate range, $\tau_{fp}^F \sim T_L$, the figure shows a maximum in $\widetilde{\epsilon}_p$, corresponding to the range for which there is the largest contribution of the QBVD to the particulate-phase kinetic energy.

Analogous to single-phase turbulence, it is possible to define an Eulerian time scale $\widetilde{\tau}_e^p$ using the kinetic energy and dissipation rate of the MEPVF, $\widetilde{\tau}_e^p = \widetilde{q}_p^2/\widetilde{\epsilon}_p$. Using (6.11) and (6.12) and the time scale $\widetilde{\tau}_e^p$, the kinetic energy of the correlated part of the particle velocity field and mean quasi-Brownian kinetic energy can be expressed as

$$\widetilde{q}_p^2 = \frac{\widetilde{\eta}_r}{1 + 2\widetilde{\eta}_r} q_{fp}, \qquad \delta q_p^2 = \frac{1}{2\widetilde{\eta}_r} \widetilde{q}_p^2. \tag{6.13}$$

In (6.13), the ratio $\widetilde{\eta}_r = \widetilde{\tau}_e^p/\tau_{fp}^F$ is introduced and characterizes the dissipation time scale of the MEPVF. As shown above (figure 9), with increases in the particle response time the quasi-Brownian component of the particle velocity field becomes relatively more dominant. The relations (6.13) show that as the contribution of the QBVD to the particulate-phase kinetic energy increases, the time-scale ratio $\widetilde{\eta}_r$ will decrease. The quantity $\widetilde{\eta}_r$ from the DNS and LES is shown in figure 13 and demonstrates that time-scale ratio in fact decreases with increases in particle response time.

6.4. *Spatial correlations and integral length scales of the MEPVF*

The influence of particle inertia on the longitudinal and lateral spatial correlations of the MEPVF is shown in figure 14. With increases in particle response time, the figure shows increasing spatial correlation in the MEPVF. The lateral components $G^{pp*}(r)$ in figure 14 show that for smaller particle response times the correlations

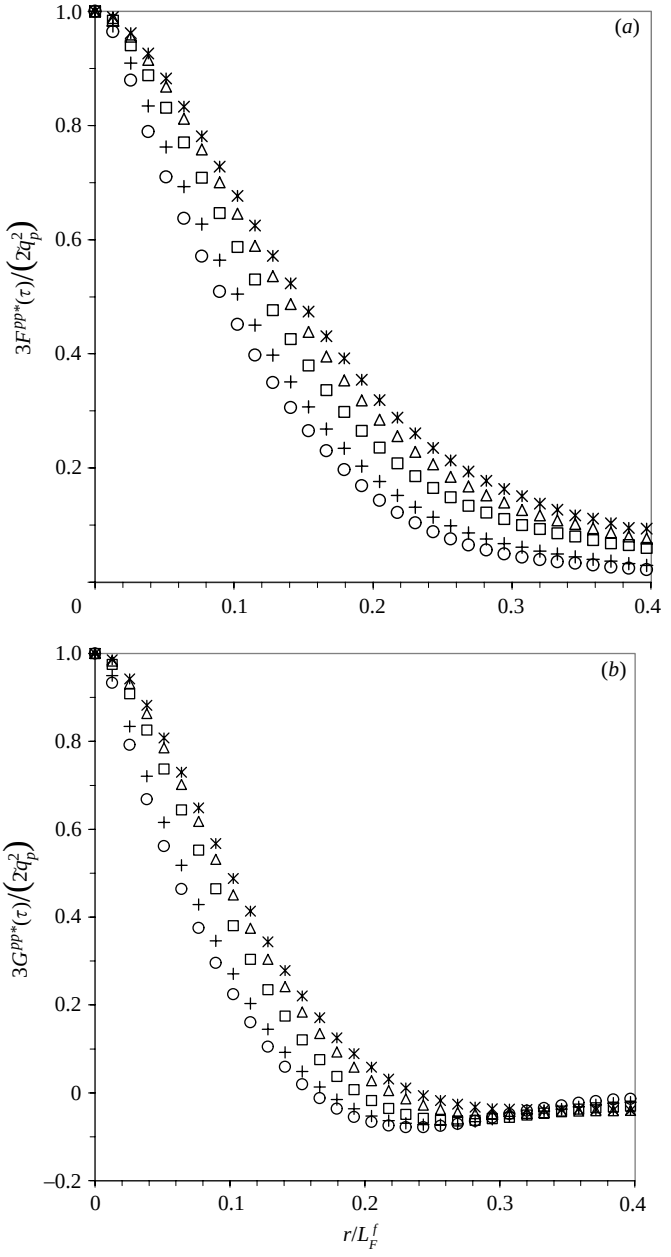

FIGURE 14. Influence of particle inertia on the Eulerian particle–particle velocity correlations, (*a*) $F^{pp*}(r)$ and (*b*) $G^{pp*}(r)$. Correlations shown from the LES at $Re_L = 700$. ○, $\tau_{fp}^F/T_L = 0.05$; +, $\tau_{fp}^F/T_L = 0.3$; □, $\tau_{fp}^F/T_L = 1.47$; △, $\tau_{fp}^F/T_L = 3.4$; *, $\tau_{fp}^F/T_L = 4.83$.

possess negative loops, consistent with the fact that the motion of these particles approaches that of fluid elements for which the negative loop is a consequence of mass conservation for incompressible flows. From the correlations shown in figure 14, including the fluid–particle spatial correlations not shown, it is possible to extract the integral length scales characterizing the MEPVF. The longitudinal integral length scales of the fluid–particle correlated motion, $\widetilde{L}_F^{fp}$, and of the MEPVF, $\widetilde{L}_F^p$, are defined

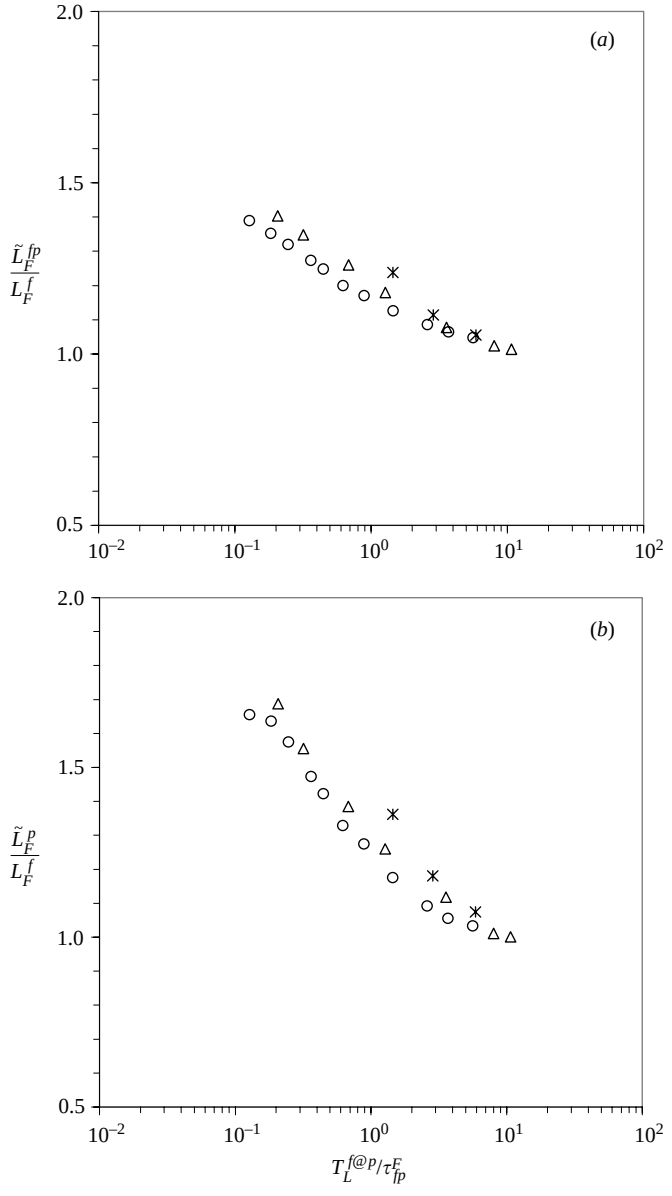

FIGURE 15. Effect of particle inertia on the integral length scales of the MEPVF, (*a*) $\widetilde{L}_F^{fp}$ and fluid–particle correlated motion, (*b*) $\widetilde{L}_F^{p}$ ○, 128^3 DNS at $Re_L = 110$; △, LES at $Re_L = 700$. ∗, Sundaram & Collins (1999).

classically as

$$\widetilde{L}_F^{fp} = \frac{1}{3}\frac{1}{q_{fp}}\int_0^\infty \widetilde{F}^{fp}(r)\,\mathrm{d}r, \qquad \widetilde{L}_F^{p} = \frac{2}{3}\frac{1}{\widetilde{q}_p^2}\int_0^\infty \widetilde{F}^{pp}(r)\,\mathrm{d}r. \tag{6.14}$$

The evolution of $\widetilde{L}_F^{fp}$ with particle inertia is depicted in figure 15. Also shown are the DNS results from Sundaram & Collins (1999). The agreement between the present calculations and those from Sundaram & Collins (1999) is adequate, both demonstrating that the longitudinal integral length scale $\widetilde{L}_F^{fp}$ increases with particle

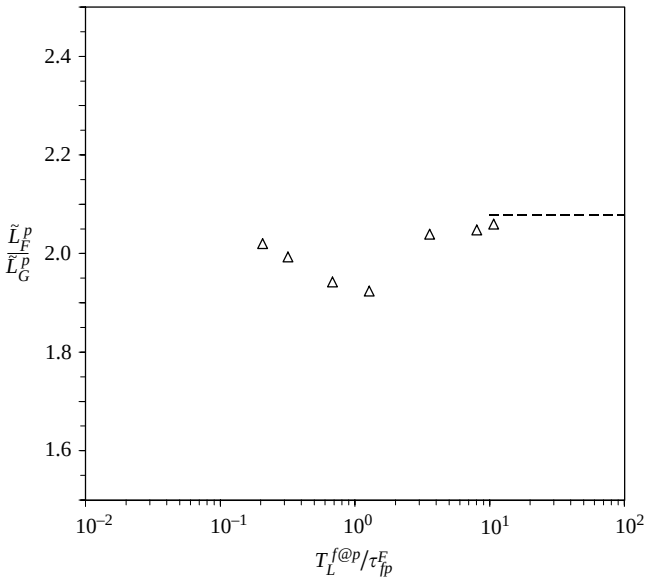

FIGURE 16. Effect of particle inertia on the integral length-scale ratio of the MEPVF, LES at $Re_L = 700$. The dashed line represents the value of the corresponding integral length-scale ratio of the fluid.

response time and indicating that the correlation between particle and fluid motions is increasingly dominated by the larger-scale motions compared to the influence of the smaller-scale fluid turbulent motions. This result is also consistent with the theoretical predictions of the spectral response by Tchen (1947), showing that particle motion will be less affected by the small-scale fluid motions for increasing particle relaxation times and that particle motion will remain correlated with the fluid scales possessing characteristic time scales larger than the response time of the particles.

The evolution of the longitudinal integral length scale of the MEPVF, $\widetilde{L}_F^p$, is shown in figure 15(*b*). The figure shows adequate agreement with the previous results of Sundaram & Collins (1999), with $\widetilde{L}_F^p$ increasing with particle response time, and also showing that the MEPVF is correlated over larger length scales compared to the fluid turbulent motions. This feature is consistent with the fact that the energy of the MEPVF decreases more rapidly at small scales than at large scales with increasing inertia. This effect can be observed via the evolution of the particle–particle velocity correlation function in figure 3, in which $3\widetilde{F}^{pp}(r)/(2q_p^2)$ does not appreciably increase for large separations compared to the relatively strong reduction of the correlation at small separations. This effect is also highlighted by the correlations $\widetilde{F}^{pp}(r)$ in figure 14. It is important to emphasize that the increase of $\widetilde{L}_F^p$ with inertia is not in contradiction with the molecular chaos limit where the velocities of separate particles are not spatially correlated. The increase in $\widetilde{L}_F^p$ with inertia reflects more the decrease of the particle–particle velocity correlation at small length scales compared to the larger scales, rather than an increase of the particle–particle velocity correlation at large length scales.

The ratio of the longitudinal to lateral integral length scales of the MEPVF is shown in figure 16. Consistent with spatial correlations discussed above, for small particle response times the ratio approaches the value of that characterizing the fluid, which is only slightly above the expectedvalue $L_F^f/L_G^f = 2$ for homogeneous isotropic

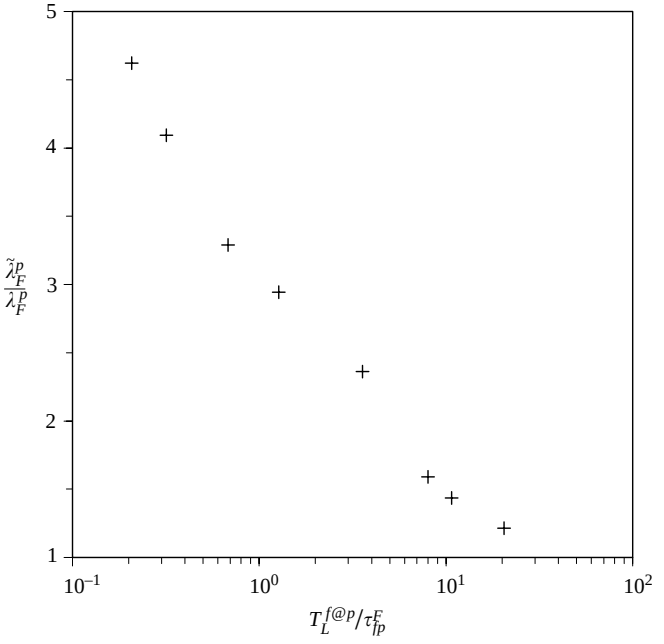

FIGURE 17. Effect of particle inertia on the 'Taylor' length scale $\widetilde{\lambda}_F^p$ of the MEPVF, LES at $Re_L = 700$.

turbulence. Interestingly, the length scale ratio in figure 16 achieves a minimum for values of the particle response time comparable to the fluid turbulence integral time scale $T_L^{f@p}$, with the coarsest particles (largest response times) showing that the ratio is again close to that characterizing the fluid flow.

6.5. *'Taylor' length scale of the MEPVF*

Figures 3 and 14 show that, in addition to the increase of the integral length scale with increasing particle inertia, there is also an increase in the length scale characterizing the particle velocity correlations for small separations, i.e. the parabolic region near the origin. To quantify such an effect the 'Taylor' length scale of the MEPVF is defined using F^{pp},

$$\widetilde{\lambda}_F^p = \left[-\frac{3}{2}\frac{1}{\widetilde{q}_p^2} \lim_{r\to 0} \frac{1}{2}\frac{\mathrm{d}^2 \widetilde{F}^{pp}(r)}{\mathrm{d}r^2} \right]^{-0.5}. \tag{6.15}$$

Note that a similar expression could be introduced for the length scale obtained from the transverse correlation function. An alternate evaluation of $\widetilde{\lambda}_F^p$ that is employed in the simulations is obtained following Laviéville (1997) by fitting using the bi-exponential function proposed by Sawford (1991) for the Lagrangian correlation in homogeneous isotropic turbulence,

$$\frac{3\widetilde{F}^{pp}(r)}{2\widetilde{q}_p^2} = \frac{\exp(-\chi^2 r/L) - \chi^2 \exp(-r/L)}{1-\chi^2}, \tag{6.16}$$

with $\widetilde{L}_F^p = L(1+1/\chi^2)$ and $\chi^2 = \sqrt{2}L/\widetilde{\lambda}_F^p$. In the limiting case of fluid elements, (6.15) and (6.16) yield values of λ_F^f $(=\widetilde{\lambda}_F^p)$ in good agreement with the expected value in homogeneous isotropic turbulence, $\lambda_F^f = \sqrt{30\nu u'^2/\epsilon}$.

The influence of particle inertia on the ratio $\widetilde{\lambda}_F^p/\lambda_F^f$, where λ_F^f is given by (6.16) for fluid elements, in figure 17 shows that the ratio increases monotonically with

increasing response time. The figure also shows that the increase in $\widetilde{\lambda}_F^p$ is larger than that occurring in the integral length scale $\widetilde{L}_F^p$. For example, for $T_L/\tau_{fp}^F \approx 0.2$, $\widetilde{L}_F^p/L_F^f \approx 1.7$ while $\widetilde{\lambda}_F^p/\widetilde{\lambda}_F^f \approx 4.6$. This characterizes the relative increase of the parabolic region of the correlation function of the MEPVF with particle inertia and should be related to the modification of the energy spectrum in the intermediate-wavenumber range.

7. Summary and conclusions

A study of the spatial characteristics of finite-inertia particle motion in gas-phase turbulent flows is presented, using both an analytical treatment and subsequent validation and investigation via numerical simulations. The current contribution considers in detail the subset of gas–particle flows in which the dispersed-phase density is much larger than that of the carrier fluid. A theoretical approach based on application of an average conditioned on a realization of the carrier fluid flow was used to develop relations governing two contributions to the velocity of a finite-inertia particle. The first contribution – the mesoscopic Eulerian particle velocity field – is a continuous velocity field shared by all the particles of the system. The remaining contribution to the particle velocity represents a random component – the quasi-Brownian velocity distribution – that accounts for the fact that a portion of the particle velocity corresponds to a distribution that is not spatially correlated, which also implies that the quasi-Brownian velocities of two neighbouring particles are not correlated. The QBVD is identified with each particle and accounts for the fact that a portion of the particle velocity obeys, partially, the assumption of molecular chaos, i.e. independence of the velocities of neighbouring particles. In the present context, the assumption of molecular chaos is restricted to the velocity distribution and not to the distribution of particle positions and also does not imply a Gaussian distribution of the velocities. In the gas–solid systems considered in this contribution, partitioning of the particle velocity into the MEPVF and QBVD is dictated by particle inertia. It was shown that the MEPVF accounts for all fluid–particle and particle–particle velocity correlations. For low-inertia particles that follow the flow, the contribution of the QBVD is not large and the particle velocities possess spatial correlations similar to that of the underlying carrier flow. With increases in particle inertia, the spatial velocity correlations are increasingly affected by the QBVD, especially for small separations.

The numerical simulations presented in the second part of the paper enabled *a posteriori* validation of the theoretical relations developed using the MEF. Both DNS and LES calculations of the fluid flow were used to assess the MEF and to gain some insight into the application of LES for extraction of the two-point spatial velocity correlations. The simulations showed good agreement in the statistics of the MEPVF and QBVD obtained using the two simulation techniques, including the changes with particle response time. These findings further support the application of LES to gas–particle flows in regimes for which the particle response time is sufficiently large compared to the smallest resolved time scales of the turbulent carrier flow, a necessary condition to ensure that subgrid velocity fluctuations in the fluid have a negligible effect on the statistics of the particulate phase. Similar findings have been reported in statistically stationary homogeneous turbulence by Boivin *et al.* (2000) and by Yamamoto *et al.* (2001) in particle-laden turbulent channel flow. In the present context, that the spatial structure of the velocity field can be captured for response times larger than the smallest resolved fluid time scales implies that application of

LES for prediction and study of problems such as the relative dispersion between particle pairs is worthwhile. It is further important to stress, however, that in other regimes, e.g. very small particle response times, the errors introduced by transporting the particulate phase by a filtered fluid velocity should be significant. More research in this area is needed to extend the parameter space amenable to accurate prediction using LES of the carrier phase for gas–solid turbulent flows.

While the existence of the MEPVF might be anticipated since particle motion is derived by interaction with an underlying turbulent fluid flow that is characterized by spatially correlated motions, the existence of the QBVD is more subtle. It is possible to envision, for example, a reduction in the kinetic energy of the correlated motions of the particulate phase occurring at the same rate as the reduction in the total kinetic energy of the dispersed phase with increasing inertia so that the QBVD is effectively zero. The simulations, however, demonstrate that the reduction in $\widetilde{q}_p^2$ occurs more rapidly than in q_p^2 with increasing particle response time, due to the transfer of energy from the MEPVF to the QBVD as shown via analysis of the transport equations of the kinetic energy and confirmed by the simulations. Other recent evidence for the partitioning of the particle velocity into spatially correlated and random-uncorrelated components is apparent in the measurements of the two-point correlations of particle velocities in fully developed turbulent channel flow reported by Khalitov & Longmire (2003), in which a discontinuity at the origin of the correlations is observed. It is also interesting to note that the statistical model of pair dispersion and preferential concentration recently presented by Zaichik & Alipchenkov (2003) predicts a discontinuity in the spatial correlations of the particle velocity.

The present contribution also has implications for calculation of particle-laden turbulent flows using Eulerian-based approaches. A simple approach that has been applied to derive the instantaneous Eulerian equations for the dispersed phase consists of volume filtering the separate, local, and instantaneous equations for each phase and then accounting for the interfacial jump conditions (Druzhinin & Elghobashi 1998). Such an approach, however, is very restrictive since particle sizes and inter-particle separations must be much smaller than the smallest length scales of the gas-phase turbulent motion. In addition, other effects such as inter-particle collisions are not easily included within such formulations.

Eulerian transport equations (6.3) and (6.4) that were developed in this work provide a new formulation for the description of particulate-phase motion that is more general than related efforts. Analysis of the transport equations and the simulations show that the evolution of the mesoscopic particle velocity interacts with the QBVD via a kinetic stress tensor that represents diffusive and pressure effects that account for the fact that into any volume Ω with dimensions comparable to or smaller than the smallest length scales of the turbulence, separate particles will possess different velocities because of separate fluid interaction histories. Eulerian-based computational approaches that attempt to resolve the time- and spatially dependent properties of the particulate phase should account for the role of the QBVD in the Eulerian particle velocity.

It should also be noted that while the transport equations for the mesoscopic field have a similar structure to those which could be obtained by volume averaging, the interpretations are not the same. Volume-averaged quantities represent the characteristics of a particular property (e.g. the particle velocity) at length scales larger than the averaging volume. Ensemble averages, on the other hand, do not impose a characteristic length scale and *a priori* are valid at all length scales. Such

an approach allows derivation of local, instantaneous equations for the dispersed phase which can be coupled with DNS of the gaseous turbulence. In addition, volume averaging of these equations may allow development of new simulation techniques, corresponding to two-fluid LES.

Solution of the momentum equation for the MEPVF requires a model for the kinetic stress and it is anticipated that the decomposition of the particle velocity obtained via the MEF will simplify modelling strategies compared to those needed in volume-averaged computations of dispersed-phase flows. Finally, in the context of classical two-fluid modelling, the transport of the particle-phase kinetic energy involves contributions from the MEPVF and QBVD. Since the MEPVF and QBVD account for very different effects governing particle motion, it might be anticipated that the MEF will improve modelling within classical two-fluid approaches.

The theoretical formalism developed in this manuscript can be extended to dilute configurations that include inter-particle collisions, assuming that particle–particle collisions do not directly induce spatial correlations in the particle velocity field. Application of the MEF is formally possible to regimes in which inter-particle collisions are included since it is based on a conditional average in terms of a given fluid flow realization. Extension of the MEF to gas–solid flows in which the carrier-phase turbulence is modified via momentum exchange with the particles is not obvious, but should be possible. For small particle diameters in gas–solid regimes, i.e. with particle response times comparable to the large eddies of the turbulent fluid flow, hydrodynamic interactions between particles should also not induce velocity correlations because of the wide separation of time scales between the particle response time and wake time scale. Formally, extension of the MEF to regimes including two-way coupling could be possible via definition of a conditional average using a single realization of the large-scale fluid flow, rather than the whole turbulent fluid velocity field as developed in this manuscript. The basis of such an approach would take advantage of the fact that for small particle diameters, the direct modification of the fluid flow occurs at very small scales. While the smallest scales over a large number of ensembles would differ from one realization to the next, the large eddies of the fluid flow would exhibit negligible variation, in turn providing the condition on which to define properties of the particulate phase.

The numerical simulations were performed on the NEC-SX5 supercomputer using time made available by the Institut du Développement et des Resources en Informatique Scientifique (IDRIS). P. F. and K. D. S. gratefully acknowledge the financial support from NASA Grant NCC-025.

Appendix. Analytical relations developed from the MEF

The averaging operator $\langle\cdot\rangle$ is defined over a large number of two-phase flow realizations,

$$\langle\cdot\rangle = \lim_{\mathscr{N}_{f\&p}\to\infty}\left[\frac{1}{\mathscr{N}_{f\&p}}\sum_{\mathscr{N}_{f\&p}}(\cdot,\mathscr{H}_{f\&p})\right] \tag{A 1}$$

where $\mathscr{N}_{f\&p}$ represents the total number of two-phase flow realizations $\mathscr{H}_{f\&p}$. Particle statistics can be derived from the p.d.f. $f_p^{(1)}$ (cf. (2.1)) as well as from the normalized version $\mathscr{F}_p^{(1)}$ (cf. (2.4)). In the following, statistical quantities are developed with respect to the normalized p.d.f., i.e. based on averaging over a very large number of

realizations of the trajectory of any given particle m of the system. The corresponding averaging operator is then expressed as

$$\frac{\left\langle \cdot\, \delta\left(\boldsymbol{x}-\boldsymbol{x}_p^{(m)}\right)\right\rangle}{\left\langle \delta\left(\boldsymbol{x}-\boldsymbol{x}_p^{(m)}\right)\right\rangle} = \left\langle \cdot\,|\boldsymbol{x}=\boldsymbol{x}_p^{(m)}\right\rangle, \tag{A 2}$$

where the right-hand side of (A 2) is a shorthand to reinforce the dependence of the average on the particle position.

In dilute systems, the fluid flow can be assumed to be undisturbed by the particle presence and it is possible to consider formally a very large number $\mathcal{N}_p$ of realizations of the particulate system for a given fluid flow realization $\mathscr{H}_f$. Each particle realization $\mathscr{H}_p$ will differ by slightly altering the particle initial conditions, possible in the current configuration of statistically stationary, homogeneous and isotropic turbulence. Statistical properties of the particulate phase can then be defined via introduction of averages conditioned on a given fluid-flow realization,

$$\langle \cdot|\mathscr{H}_f\rangle = \lim_{\mathcal{N}_p\to\infty}\left[\frac{1}{\mathcal{N}_p}\sum_{\mathcal{N}_p}(\cdot,\mathscr{H}_p|\mathscr{H}_f)\right], \tag{A 3}$$

from which follows

$$\langle\cdot\rangle = \lim_{\mathcal{N}_f\to\infty}\left[\frac{1}{\mathcal{N}_f}\sum_{\mathcal{N}_f}\langle\cdot|\mathscr{H}_f\rangle\right]. \tag{A 4}$$

For ease of notation, the relation (A 4) is written more compactly as,

$$\langle\cdot\rangle = \left\{\langle\cdot|\mathscr{H}_f\rangle\right\}_f, \qquad \text{with} \qquad \{\cdot\}_f = \lim_{\mathcal{N}_f\to\infty}\left[\frac{1}{\mathcal{N}_f}\sum_{\mathcal{N}_f}(\cdot,\mathscr{H}_f)\right].$$

According to the idempotence (identity) property of the averaging operator, i.e. $\langle\langle\cdot\rangle\rangle = \langle\cdot\rangle$, the following relation holds:

$$\langle\langle\cdot|\mathscr{H}_f\rangle\rangle = \left\{\langle\langle\cdot|\mathscr{H}_f\rangle|\mathscr{H}_f\rangle\right\}_f = \left\{\langle\cdot|\mathscr{H}_f\rangle\right\}_f = \langle\cdot\rangle. \tag{A 5}$$

A.1. *Relations between one-point statistics*

In the MEF, the velocity $\widetilde{\boldsymbol{v}}_p$ is defined as

$$\begin{aligned}\widetilde{\boldsymbol{v}}_p(\boldsymbol{x},t,\mathscr{H}_f) &= \frac{\left\langle \boldsymbol{v}_p^{(m)}(t)\delta\left(\boldsymbol{x}-\boldsymbol{x}_p^{(m)}\right)\middle|\mathscr{H}_f\right\rangle}{\left\langle \delta\left(\boldsymbol{x}-\boldsymbol{x}_p^{(m)}\right)\middle|\mathscr{H}_f\right\rangle}\\ &= \left\langle \boldsymbol{v}_p^{(m)}(t)|\boldsymbol{x}=\boldsymbol{x}_p^{(m)};\mathscr{H}_f\right\rangle,\end{aligned}$$

where the second line is again a more compact representation of the average, also indicating the dependence on $\mathscr{H}_f$. The velocities $\widetilde{\boldsymbol{v}}_p$ and $\boldsymbol{\delta v}_p$ are related to the velocity of particle m as

$$\boldsymbol{v}_p^{(m)}(t) = \widetilde{\boldsymbol{v}}_p\left(\boldsymbol{x}_p^{(m)}(t),t,\mathscr{H}_f\right) + \boldsymbol{\delta v}_p^{(m)}(t).$$

Using (A 5), the following relations can be derived for the statistics of the velocities $\boldsymbol{v}_p$, $\widetilde{\boldsymbol{v}}_p$, and $\boldsymbol{\delta v}_p$. For the mean particle velocity $\boldsymbol{V}_p(x,t) = \langle \boldsymbol{v}_p^{(m)}(t)|\boldsymbol{x}=\boldsymbol{x}_p^{(m)}(t)\rangle$,

$$\begin{aligned}\boldsymbol{V}_p(\boldsymbol{x},t) &= \left\langle \widetilde{\boldsymbol{v}}_p(\boldsymbol{x},t,\mathscr{H}_f) + \boldsymbol{\delta v}_p^{(m)}(t)|\boldsymbol{x}=\boldsymbol{x}_p^{(m)}(t)\right\rangle\\ &= \left\langle \widetilde{\boldsymbol{v}}_p(\boldsymbol{x},t,\mathscr{H}_f)|\boldsymbol{x}=\boldsymbol{x}_p^{(m)}(t)\right\rangle + \left\langle \boldsymbol{\delta v}_p^{(m)}(t)|\boldsymbol{x}=\boldsymbol{x}_p^{(m)}(t)\right\rangle\end{aligned}$$

$$= \left\langle \widetilde{\boldsymbol{v}}_p(\boldsymbol{x}, t, \mathscr{H}_f)|\boldsymbol{x} = \boldsymbol{x}_p^{(m)}(t)\right\rangle + \left\langle \left\langle \boldsymbol{\delta v}_p^{(m)}(t)|\boldsymbol{x} = \boldsymbol{x}_p^{(m)}(t); \mathscr{H}_f\right\rangle\right\rangle$$
$$= \left\langle \widetilde{\boldsymbol{v}}_p(\boldsymbol{x}, t, \mathscr{H}_f)|\boldsymbol{x} = \boldsymbol{x}_p^{(m)}(t)\right\rangle, \tag{A 6}$$

since the average $\langle \boldsymbol{\delta v}_p^{(m)}(t)|x = x_p^{(m)}(t); \mathscr{H}_f\rangle \equiv 0$. Furthermore, the last line of (A 6) can be simplified using the average (A 2) and property (A 5),

$$\left\langle \widetilde{\boldsymbol{v}}_p(\boldsymbol{x}, t, \mathscr{H}_f)|\boldsymbol{x} = \boldsymbol{x}_p^{(m)}(t)\right\rangle = \frac{\left\langle \widetilde{\boldsymbol{v}}_p(\boldsymbol{x}, t, \mathscr{H}_f)\delta\left(\boldsymbol{x} - \boldsymbol{x}_p^{(m)}(t)\right)\right\rangle}{\left\langle \delta\left(\boldsymbol{x} - \boldsymbol{x}_p^{(m)}(t)\right)\right\rangle}$$
$$= \frac{\left\langle \left\langle \widetilde{\boldsymbol{v}}_p(\boldsymbol{x}, t, \mathscr{H}_f)\delta\left(\boldsymbol{x} - \boldsymbol{x}_p^{(m)}(t)\right)|\mathscr{H}_f\right\rangle\right\rangle}{\left\langle \left\langle \delta\left(\boldsymbol{x} - \boldsymbol{x}_p^{(m)}(t)\right)|\mathscr{H}_f\right\rangle\right\rangle}$$
$$= \frac{\left\langle \widetilde{\boldsymbol{v}}_p(\boldsymbol{x}, t, \mathscr{H}_f)\left\langle \delta\left(\boldsymbol{x} - \boldsymbol{x}_p^{(m)}(t)\right)|\mathscr{H}_f\right\rangle\right\rangle}{\left\langle \left\langle \delta\left(\boldsymbol{x} - \boldsymbol{x}_p^{(m)}(t)\right)|\mathscr{H}_f\right\rangle\right\rangle}$$
$$= \frac{\left\langle \widetilde{\boldsymbol{v}}_p(\boldsymbol{x}, t, \mathscr{H}_f)\widetilde{n}_p(\boldsymbol{x}, t, \mathscr{H}_f)\right\rangle}{\left\langle \widetilde{n}_p(\boldsymbol{x}, t, \mathscr{H}_f)\right\rangle} = \widetilde{\boldsymbol{V}}_p(\boldsymbol{x}, t), \tag{A 7}$$

where $\widetilde{\boldsymbol{V}}_p$ is the density-weighted mean velocity. The relations (A 6) and (A 7) show that the mean particle velocity and density-weighted value are identical. The fluctuating velocity of any particle can then be expressed as

$$\boldsymbol{v}'^{(m)}_p(t) = \boldsymbol{v}_p^{(m)}(t) - \boldsymbol{V}_p\left(\boldsymbol{x}_p^{(m)}(t), t\right)$$
$$= \widetilde{\boldsymbol{v}}_p\left(\boldsymbol{x}_p^{(m)}(t), t, \mathscr{H}_f\right) + \boldsymbol{\delta v}_p^{(m)}(t) - \boldsymbol{V}_p\left(\boldsymbol{x}_p^{(m)}(t), t\right)$$
$$= \widetilde{\boldsymbol{v}}'_p\left(\boldsymbol{x}_p^{(m)}(t), t, \mathscr{H}_f\right) + \boldsymbol{\delta v}_p^{(m)}(t). \tag{A 8}$$

The total turbulent kinetic energy of the particulate phase can be expressed in terms of $\widetilde{\boldsymbol{v}}'_p$ and $\boldsymbol{\delta v}_p$ (note that the dependence of these quantities on $\boldsymbol{x}$, t and $\mathscr{H}_f$ is not explicitly indicated in the following relations):

$$q_p^2(\boldsymbol{x}, t) = \tfrac{1}{2}\left\langle v'^{(m)2}_{p,i}\middle|\boldsymbol{x} = \boldsymbol{x}_p^{(m)}\right\rangle$$
$$= \tfrac{1}{2}\left\langle \left(\widetilde{v}'_{p,i} + \delta v_{p,i}^{(m)}\right)^2\middle|\boldsymbol{x} = \boldsymbol{x}_p^{(m)}\right\rangle$$
$$= \tfrac{1}{2}\left\langle \widetilde{v}'^{\,2}_{p,i}\middle|\boldsymbol{x} = \boldsymbol{x}_p^{(m)}\right\rangle + \left\langle \widetilde{v}'_{p,i}\delta v_{p,i}^{(m)}\middle|\boldsymbol{x} = \boldsymbol{x}_p^{(m)}\right\rangle + \tfrac{1}{2}\left\langle \delta v_{p,i}^{(m)2}\middle|\boldsymbol{x} = \boldsymbol{x}_p^{(m)}\right\rangle$$

The second term on the right-hand side can be simplified,

$$\left\langle \widetilde{v}'_{p,i}\delta v_{p,i}^{(m)}\middle|\boldsymbol{x} = \boldsymbol{x}_p^{(m)}\right\rangle = \left\langle \left\langle \widetilde{v}'_{p,i}\delta v_{p,i}^{(m)}\middle|\boldsymbol{x} = \boldsymbol{x}_p^{(m)}; \mathscr{H}_f\right\rangle\right\rangle$$
$$= \left\langle \widetilde{v}'_{p,i}\left\langle \delta v_{p,i}^{(m)}\middle|\boldsymbol{x} = \boldsymbol{x}_p^{(m)}; \mathscr{H}_f\right\rangle\right\rangle = 0,$$

and thus the total turbulent kinetic energy of the particles can be expressed as

$$q_p^2(\boldsymbol{x}, t) = \widetilde{q}_p^2(\boldsymbol{x}, t) + \delta q_p^2(\boldsymbol{x}, t) \tag{A 9}$$

where,

$$\widetilde{q}_p^2(\boldsymbol{x}, t) = \frac{1}{2}\left\langle \widetilde{v}'^2_{p,i}(\boldsymbol{x}, t, \mathscr{H}_f)\middle|\boldsymbol{x} = \boldsymbol{x}_p^{(m)}(t)\right\rangle$$
$$= \frac{1}{2}\frac{\left\langle \widetilde{n}_p(\boldsymbol{x}, t, \mathscr{H}_f)\widetilde{v}'^2_{p,i}(\boldsymbol{x}, t, \mathscr{H}_f)\right\rangle}{\left\langle \widetilde{n}_p(\boldsymbol{x}, t, \mathscr{H}_f)\right\rangle} \tag{A 10}$$

in which the second line above follows in the same way as that leading to (A 7), and

$$\delta q_p^2(\boldsymbol{x}, t) = \tfrac{1}{2}\left\langle \delta v_{p,i}^{(m)2}(t)\middle|\boldsymbol{x} = \boldsymbol{x}_p^{(m)}(t)\right\rangle. \tag{A 11}$$

The fluid–particle velocity covariance is expressed as

$$q_{fp}(\boldsymbol{x},t)=\left\langle u_i'\widetilde{v}_{p,i}'\middle|\boldsymbol{x}=\boldsymbol{x}_p^{(m)}\right\rangle+\left\langle u_i'\delta v_{p,i}^{(m)}\middle|\boldsymbol{x}=\boldsymbol{x}_p^{(m)}\right\rangle.$$

Furthermore,

$$\left\langle u_i'\delta v_{p,j}^{(m)}\middle|x=x_p^{(m)}\right\rangle=\left\langle u_i\left\langle\delta v_{p,j}^{(m)}\middle|x=x_p^{(m)};\mathscr{H}_f\right\rangle\right\rangle=0.$$

The above shows that the velocity $\boldsymbol{\delta v}_p$ of any particle is not correlated with the fluid velocity at the particle position. This in turn shows that the instantaneous Eulerian particle velocity $\widetilde{\boldsymbol{v}}_p$ takes completely into account the fluid–particle one-point velocity correlations, i.e.

$$q_{fp}(\boldsymbol{x},t)=\widetilde{q}_{fp}(\boldsymbol{x},t). \tag{A 12}$$

Using the same approach, it can be shown that the fluid kinetic energy sampled along particle trajectories satisfies an analogous relation, i.e.

$$q_{f@p}^2(\boldsymbol{x},t)=\widetilde{q}_{f@p}^2(\boldsymbol{x},t). \tag{A 13}$$

A.2. *Relations between two-point statistics*

Statistical relationships for the two-point Eulerian statistics of the particulate phase derived from consideration of the centres of two different particles m and n are developed in this subsection. The radial distribution function g^{pp} takes the form

$$\begin{aligned}g^{pp}(\boldsymbol{x},\boldsymbol{x}+\boldsymbol{r},t)&=\frac{\left\langle\delta\left(\boldsymbol{x}-\boldsymbol{x}_p^{(m)}\right)\delta\left(\boldsymbol{x}+\boldsymbol{r}-\boldsymbol{x}_p^{(n)}\right)\right\rangle}{\left\langle\delta\left(\boldsymbol{x}-\boldsymbol{x}_p^{(m)}\right)\right\rangle\left\langle\delta\left(\boldsymbol{x}+\boldsymbol{r}-\boldsymbol{x}_p^{(n)}\right)\right\rangle}\\&=\frac{\left\langle\left\langle\delta\left(\boldsymbol{x}-\boldsymbol{x}_p^{(m)}\right)\delta\left(\boldsymbol{x}+\boldsymbol{r}-\boldsymbol{x}_p^{(n)}\right)\middle|\mathscr{H}_f\right\rangle\right\rangle}{\left\langle\left\langle\delta\left(\boldsymbol{x}-\boldsymbol{x}_p^{(m)}\right)\middle|\mathscr{H}_f\right\rangle\right\rangle\left\langle\left\langle\delta\left(\boldsymbol{x}+\boldsymbol{r}-\boldsymbol{x}_p^{(n)}\right)\middle|\mathscr{H}_f\right\rangle\right\rangle}\\&=\frac{\left\langle\left\langle\delta\left(\boldsymbol{x}-\boldsymbol{x}_p^{(m)}\right)\middle|\mathscr{H}_f\right\rangle\left\langle\delta\left(\boldsymbol{x}+\boldsymbol{r}-\boldsymbol{x}_p^{(n)}\right)\middle|\mathscr{H}_f\right\rangle\right\rangle}{\left\langle\left\langle\delta\left(\boldsymbol{x}-\boldsymbol{x}_p^{(m)}\right)\middle|\mathscr{H}_f\right\rangle\right\rangle\left\langle\left\langle\delta\left(\boldsymbol{x}+\boldsymbol{r}-\boldsymbol{x}_p^{(n)}\right)\middle|\mathscr{H}_f\right\rangle\right\rangle}\\&=\frac{\langle\widetilde{n}_p(\boldsymbol{x},t,\mathscr{H}_f)\widetilde{n}_p(\boldsymbol{x}+\boldsymbol{r},t,\mathscr{H}_f)\rangle}{\langle\widetilde{n}_p(\boldsymbol{x},t,\mathscr{H}_f)\rangle\langle\widetilde{n}_p(\boldsymbol{x}+\boldsymbol{r},t,\mathscr{H}_f)\rangle}.\end{aligned} \tag{A 14}$$

The particle–particle velocity correlation can be written as

$$\begin{aligned}R_{ij}^{pp}(\boldsymbol{x},\boldsymbol{x}+\boldsymbol{r},t)&=\left\langle v_{p,i}'^{(m)}v_{p,j}'^{(n)}\middle|\boldsymbol{x}=\boldsymbol{x}_p^{(m)};\boldsymbol{x}+\boldsymbol{r}=\boldsymbol{x}_p^{(n)}\right\rangle\\&=\frac{\left\langle v_{p,i}'^{(m)}v_{p,j}'^{(n)}\delta\left(\boldsymbol{x}-\boldsymbol{x}_p^{(m)}\right)\delta\left(\boldsymbol{x}+\boldsymbol{r}-\boldsymbol{x}_p^{(n)}\right)\right\rangle}{\left\langle\delta\left(\boldsymbol{x}-\boldsymbol{x}_p^{(m)}\right)\delta\left(\boldsymbol{x}+\boldsymbol{r}-\boldsymbol{x}_p^{(n)}\right)\right\rangle}.\end{aligned} \tag{A 15}$$

Using the decomposition (A 8), the correlations can be re-written as

$$\begin{aligned}&R_{ij}^{pp}(\boldsymbol{x},\boldsymbol{x}+\boldsymbol{r})\\&=\frac{1}{\left\langle\delta\left(\boldsymbol{x}-\boldsymbol{x}_p^{(m)}\right)\delta\left(\boldsymbol{x}+\boldsymbol{r}-\boldsymbol{x}_p^{(n)}\right)\right\rangle}\left[\left\langle\widetilde{v}_{p,i}'(\boldsymbol{x})\widetilde{v}_{p,j}'(\boldsymbol{x}+\boldsymbol{r})\delta\left(\boldsymbol{x}-\boldsymbol{x}_p^{(m)}\right)\delta\left(\boldsymbol{x}+\boldsymbol{r}-\boldsymbol{x}_p^{(n)}\right)\right\rangle\right.\\&\quad+\left\langle\widetilde{v}_{p,i}'(\boldsymbol{x})\delta v_{p,j}^{(n)}\delta\left(\boldsymbol{x}-\boldsymbol{x}_p^{(m)}\right)\delta\left(\boldsymbol{x}+\boldsymbol{r}-\boldsymbol{x}_p^{(n)}\right)\right\rangle\\&\quad+\left\langle\delta v_{p,i}^{(m)}\widetilde{v}_{p,j}'(\boldsymbol{x}+\boldsymbol{r})\delta\left(\boldsymbol{x}-\boldsymbol{x}_p^{(m)}\right)\delta\left(\boldsymbol{x}+\boldsymbol{r}-\boldsymbol{x}_p^{(n)}\right)\right\rangle\\&\quad\left.+\left\langle\delta v_{p,i}^{(m)}\delta v_{p,j}^{(n)}\delta\left(\boldsymbol{x}-\boldsymbol{x}_p^{(m)}\right)\delta\left(\boldsymbol{x}+\boldsymbol{r}-\boldsymbol{x}_p^{(n)}\right)\right\rangle\right].\end{aligned} \tag{A 16}$$

Note that the dependence on t and $\mathscr{H}_f$ is not explicitly indicated in the above. The first term on the right-hand side above can be expressed as

$$\begin{aligned}
&\langle \widetilde{v}'_{p,i}(\boldsymbol{x})\widetilde{v}'_{p,j}(\boldsymbol{x}+\boldsymbol{r})\delta\big(\boldsymbol{x}-\boldsymbol{x}_p^{(m)}\big)\delta\big(\boldsymbol{x}+\boldsymbol{r}-\boldsymbol{x}_p^{(n)}\big)\rangle \\
&\quad=\big\langle\big\langle \widetilde{v}'_{p,i}(\boldsymbol{x})\widetilde{v}'_{p,j}(\boldsymbol{x}+\boldsymbol{r})\delta\big(\boldsymbol{x}-\boldsymbol{x}_p^{(m)}\big)\delta\big(\boldsymbol{x}+\boldsymbol{r}-\boldsymbol{x}_p^{(n)}\big)\big|\mathscr{H}_f\big\rangle\big\rangle \\
&\quad=\big\langle \widetilde{v}'_{p,i}(\boldsymbol{x})\widetilde{v}'_{p,j}(\boldsymbol{x}+\boldsymbol{r})\big\langle\delta\big(\boldsymbol{x}-\boldsymbol{x}_p^{(m)}\big)\delta\big(\boldsymbol{x}+\boldsymbol{r}-\boldsymbol{x}_p^{(n)}\big)\big|\mathscr{H}_f\big\rangle\big\rangle \\
&\quad=\big\langle \widetilde{v}'_{p,i}(\boldsymbol{x})\widetilde{v}'_{p,j}(\boldsymbol{x}+\boldsymbol{r})\big\langle\delta\big(\boldsymbol{x}-\boldsymbol{x}_p^{(m)}\big)\big|\mathscr{H}_f\big\rangle\big\langle\delta\big(\boldsymbol{x}+\boldsymbol{r}-\boldsymbol{x}_p^{(n)}\big)\big|\mathscr{H}_f\big\rangle\big\rangle.
\end{aligned}$$

The second term on the right-hand side can be expressed as

$$\begin{aligned}
&\langle \widetilde{v}'_{p,i}(\boldsymbol{x})\delta v_{p,j}^{(n)}\delta\big(\boldsymbol{x}-\boldsymbol{x}_p^{(m)}\big)\delta\big(\boldsymbol{x}+\boldsymbol{r}-\boldsymbol{x}_p^{(n)}\big)\rangle \\
&\quad=\big\langle\big\langle \widetilde{v}'_{p,i}(\boldsymbol{x})\delta v_{p,j}^{(n)}\delta\big(\boldsymbol{x}-\boldsymbol{x}_p^{(m)}\big)\delta\big(\boldsymbol{x}+\boldsymbol{r}-\boldsymbol{x}_p^{(n)}\big)\big|\mathscr{H}_f\big\rangle\big\rangle \\
&\quad=\big\langle \widetilde{v}'_{p,i}(\boldsymbol{x})\big\langle\delta\big(\boldsymbol{x}-\boldsymbol{x}_p^{(m)}\big)|\mathscr{H}_f\big\rangle\big\langle\delta v_{p,j}^{(n)}\delta\big(\boldsymbol{x}+\boldsymbol{r}-\boldsymbol{x}_p^{(n)}\big)\big|\mathscr{H}_f\big\rangle\big\rangle=0. \qquad \text{(A 17)}
\end{aligned}$$

Furthermore, using the same approach it can also be shown that the third and fourth terms on the right-hand side of (A 16) are identically zero. Consequently, the following relation is obtained:

$$\begin{aligned}
R_{ij}^{pp}(\boldsymbol{x},\boldsymbol{x}+\boldsymbol{r}) &= \frac{\big\langle \widetilde{v}'_{p,i}(\boldsymbol{x})\widetilde{v}'_{p,j}(\boldsymbol{x}+\boldsymbol{r})\big\langle\delta\big(\boldsymbol{x}-\boldsymbol{x}_p^{(m)}\big)\big|\mathscr{H}_f\big\rangle\big\langle\delta\big(\boldsymbol{x}+\boldsymbol{r}-\boldsymbol{x}_p^{(n)}\big)\big|\mathscr{H}_f\big\rangle\big\rangle}{\big\langle\big\langle\delta\big(\boldsymbol{x}-\boldsymbol{x}_p^{(m)}\big)\big|\mathscr{H}_f\big\rangle\big\langle\delta\big(\boldsymbol{x}+\boldsymbol{r}-\boldsymbol{x}_p^{(n)}\big)\big|\mathscr{H}_f\big\rangle\big\rangle} \\
&= \frac{\big\langle \widetilde{n}_p(\boldsymbol{x})\widetilde{v}_p(\boldsymbol{x})\widetilde{n}_p(\boldsymbol{x}+\boldsymbol{r})\widetilde{v}_p(\boldsymbol{x}+\boldsymbol{r})\big\rangle}{\big\langle \widetilde{n}_p(\boldsymbol{x})\widetilde{n}_p(\boldsymbol{x}+\boldsymbol{r})\big\rangle} \\
&= \widetilde{R}_{ij}^{pp}(\boldsymbol{x},\boldsymbol{x}+\boldsymbol{r}). \qquad \text{(A 18)}
\end{aligned}$$

The same approach yields analogous relations for the fluid–particle velocity correlations, R_{ij}^{fp} and $\widetilde{R}_{ij}^{fp}$ and fluid–fluid velocity correlations R_{ij}^{ff} and $\widetilde{R}_{ij}^{ff}$.

REFERENCES

Abrahamson, J. 1975 Collision rates of small particles in a vigorously turbulent fluid. *Chem. Engng Sci.* **30**, 1371–1379.

Balachandar, S. & Maxey, M. R. 1989 Methods for evaluating fluid velocities in spectral simulations of turbulence. *J. Comput. Phys.* **83**, 96–125.

Boivin, M., Simonin, O. & Squires, K. D. 1998 Direct numerical simulation of turbulence modulation by particles in isotropic turbulence. *J. Fluid Mech.* **375**, 235–263.

Boivin, M., Simonin, O. & Squires, K. D. 2000 On the prediction of gas–solid flows with two-way coupling using large eddy simulation. *Phys. Fluids* **12**, 2080–2090.

Calmet, I. & Magnaudet, J. 1997 Large-Eddy Simulation of high-Schmidt-number mass transfer in a turbulent channel flow. *Phys. Fluids* **9**, 438–455.

Deutsch, E. & Simonin, O. 1991 Large eddy simulation applied to the motion of particles in stationary homogeneous fluid turbulence. In *Turbulence Modification in Multiphase Flow*. ASME–FED, vol. 110, pp. 35–42.

Druzhinin, O. A. & Elghobashi, S. E. 1998 Direct numerical simulations of bubble-laden turbulent flows using the two-fluid formulation. *Phys. Fluids* **10**, 685–697.

Elghobashi, S. E. & Truesdell, G. C. 1993 On the two-way interaction between homogeneous turbulence and dispersed solid particles. I: turbulence modification. *Phys. Fluids* A **5**, 1790.

Eswaran, V. & Pope, S. B. 1988 An examination of forcing in direct numerical simulations of turbulence. *Computers Fluids* **16**, 257–278.

Falkovich, G., Gawedzki, K. & Vergassola, M. 2001 Particles and fluids in fluid turbulence. *Rev. Mod. Phys.* **73**, 913–975.

Février, P. 2000 Etude numérique des effets de concentration preférentielle et de corrélation spatiale entre vitesses de particules solides en turbulence homogène isotrope stationnaire. PhD Thesis, INPT/ENSEEIHT, Toulouse, France.

Hinze, J. O. 1975 *Turbulence*. McGraw-Hill.

Khalitov, D. A. & Longmire, E. K. 2003 Effect of particle size on velocity correlations in turbulent channel flow. *Proc. 4th ASME/JSME Joint Fluids Engineering conf. Honolulu, HI, 2003*. FEDSM03-45730 (available on CD).

Kraichnan, R. 1970 Diffusion by a random velocity field. *Phys. Fluids* **13**, 22–31.

Laviéville, J. 1997 Simulation numériques et modélisation des interactions entre l'entrainement par la turbulence et les collisions interparticulaires en écoulements gaz-solide. PhD Thesis, Université de Rouen, France.

Laviéville, J., Deutsch, E. & Simonin, O. 1995 Large eddy simulation of interaction between colliding particles and a homogeneous isotropic turbulent field. *6th Symp. on Gas–Solid Flows*. ASME FED, vol. 228, pp. 347–357.

Maxey, M. R. 1987 The gravitational settling of aerosol particles in homogeneous turbulence and random flow fields. *J. Fluid Mech.* **174**, 441–465.

Maxey, M. R. & Riley, J. 1983 Equation of motion of a small rigid sphere in a nonuniform flow. *Phys. Fluids* **26**, 883–889.

Pismen, L. M. & Nir, A. 1978 On the motion of suspended particles in stationary homogeneous turbulence. *J. Fluid Mech.* **84**, 193–206.

Reade, W. C. & Collins, L. R. 2000 Effect of preferential concentration on turbulent collision rates. *Phys. Fluids* **12**, 2530–2540.

Reeks, M. W. 1977 On the dispersion of small particles suspended in an isotropic turbulent field. *J. Fluid Mech.* **83**, 529–546.

Reeks, M. W. 1991 On a kinetic equation for the transport of particles in turbulent flows. *Phys. Fluids* A **3**, 446–456.

Saffman, P. G. & Turner, J. S. 1956 On the collision of drops in turbulent clouds. *J. Fluid Mech.* **1**, 16–30.

Sawford, B. L. 1991 Reynolds number effects in Lagrangian stochastic models of turbulent dispersion. *Phys. Fluids* A **3**, 1577–1590.

Schiller, L. & Nauman, A. 1935 A drag coefficient correlation. *V.D.I. Zeitung* **77**, 318–320.

Simonin, O. 1991 Prediction of the dispersed phase turbulence in particulate laden jet. *Proc. 4th Intl Symp. on Gas-Solid Flows*. ASME FED, vol. 121, pp. 197–206.

Simonin, O., Deutsch, E. & Boivin, M. 1995 Comparison of large-eddy simulation and second-moment closure of particle fluctuating motion in two-phase turbulent shear flows. *Turbulent Shear Flows 9* (ed. F. Durst *et al.*), pp. 85–115, Springer.

Sommerfeld, M. 2000 Theoretical and experimental modeling of particulate flow: overview and fundamentals. *VKI for Fluid Dynamics*. Lecture Series 2000–06.

Squires, K. D. & Eaton, J. K. 1990 Particle response and turbulence modification in isotropic turbulence. *Phys. Fluids* A **2**, 1191–1203.

Squires, K. D. & Eaton, J. K. 1991*a* Preferential concentration of particles by turbulence. *Phys. Fluids* A **3**, 1169–1178.

Squires, K. D. & Eaton, J. K. 1991*b* Measurements of particle dispersion from direct numerical simulations of isotropic turbulence. *J. Fluid Mech.* **226**, 1–35.

Sundaram, S. & Collins, L. R. 1994 Spectrum of density fluctuations in a particle-fluid system. I. monodisperse spheres. *Intl J. Multiphase Flows* **20**, 1021–1037.

Sundaram, S. & Collins, L. R. 1997 Collision statistics in an isotropic particle-laden turbulent suspension. Part 1. Direct numerical simulations. *J. Fluid Mech.* **335**, 75–109.

Sundaram, S. & Collins, L. R. 1999 A numerical study of the modulation of isotropic turbulence by suspended particles. *J. Fluid Mech.* **379**, 105–143.

Tchen, C. M. 1947 Mean value and correlation problems connected with the motion of small particles suspended in a turbulent fluid. PhD thesis, University of Delft, The Hague.

Wang, L. P., Burton, T. D. & Stock, D. E. 1990 Chaotic dynamics of heavy particle dispersion: Fractal dimension versus dispersion coefficients. *Phys. Fluids* A **2**, 1305–1308.

Wang, L. P., Burton, T. D. & Stock, D. E. 1991 Quantification of chaotic dynamics for heavy particle dispersion in ABC flow. *Phys. Fluids* A **3**, 1073–1080.

Wang, L. P. & Maxey, M. R. 1993 Settling velocity and concentration distribution of heavy particles in homogeneous isotropic turbulence. *J. Fluid Mech.* **256**, 27–68.

Wang, L. P., Wexler, A. S. & Zhou, Y. 2000 Statistical mechanical description and modelling of turbulent collision of inertial particles. *J. Fluid Mech.* **415**, 117–153.

Wang, Q. & Squires, K. 1996 Large eddy simulation of particle-laden turbulent channel flow. *Phys. Fluids* **8**, 1207–1223.

Yamamoto, Y., Potthoff, M., Tanaka, T., Kajishima, T. & Tsuji, Y. 2001 Large-eddy simulation of turbulence gas-particle flow in a vertical channel: effect of considering inter-particle collisions. *J. Fluid Mech.* **442**, 303–334.

Yeh, F. & Lei, U. 1991 On the motion of small particles in a homogeneous isotropic turbulent flow. *Phys. Fluids* A **3**, 2571–2586.

Yeung, P. K. & Pope, S. B. 1989 Lagrangian statistics from direct numerical simulations of isotropic turbulence. *J. Fluid Mech.* **207**, 531–586.

Zaichik, L. I. & Alipchenkov, V. M. 2003 Pair dispersion and preferential concentration of particles in isotropic turbulence. *Phys. Fluids* **15**, 1776–1787.

Zang, Y., Street, R. L. & Koseff, J. R. 1993 A dynamic mixed subgrid-scale model and its application to turbulent recirculating flows. *Phys. Fluids* A **5**, 3186.